Review Article

Atomically dispersed materials: Ideal catalysts in atomic era

Tao Gan and Dingsheng Wang (✉)

Department of Chemistry, Tsinghua University, Beijing 100084, China

ABSTRACT

Catalysts can accelerate the chemical reaction rate and effectively promote the molecules transformation, which is of great significance in the research of chemical industry and material science. The extreme utilization of reactive sites has led to the emergence and development of atomically dispersed materials (ADMs). The highly active coordination unsaturated metal sites and fully utilized metal atoms make ADMs show great potential in catalytic reactions. The adjustment of coordination environment and electronic structure provides more possibilities for constructing reactive centers with different properties. This review summarized the application and research progress of ADMs in different fields. The design strategy and structure–activity relationship of ADMs for specific reactions were summarized and analyzed. Moreover, we also provided advices for the challenges and opportunities faced by ADMs in catalytic reactions.

KEYWORDS

atomically dispersed materials, catalysis, organic synthesis, battery, sensor, enzyme

1   Introduction

Catalysis is the cornerstone of chemical industry and of great significance in material science research. About 90% of chemicals are produced involving catalysts during the manufacture [1]. For example, the Haber–Bosch process was applied into the synthetic ammonia industry [2]. The Ziegler–Natta catalysts can be used to produce various plastics [3]. The three-way catalyst (TWC) solves the pollution of automobile exhaust [4]. In fact, numerous cases can reflect the importance of catalysis beyond the examples listed above. Today, new catalysts and new catalytic technologies are constantly promoting the development and technological progress of chemical industry. At the same time, catalysis will also play an important role in dealing with energy and environmental crises in modern society.

The improvement of activity and stability is the eternal pursuit for catalyst development. It requires us to have a clear understanding of the reaction mechanism. The adsorption and activation of reactant molecules on the active sites are the prerequisites for catalytic reaction. The formed intermediate further converted into the products and desorbed to renew the active center. During the reaction, the exposed atoms of catalysts are the effective reactive centers. The bulk atoms are likely to be useless. Increasing the surface atomic proportion of metal sites of catalyst can be an effective strategy to improve the catalytic efficiency [5]. For example, reducing the metal particle size and increasing the dispersion can effectively increase the surface exposed metal atomic sites. In the past years, researchers prepared a great deal of industry catalysts by dispersing the active component on high surface area supports including Al_2O_3 [6–8], SiO_2 [9], zeolites [10–12], and carbon materials [13–21]. The extreme of active components dispersion is to form the isolated metal sites, which is so-called the atomically dispersed materials

(ADMs). ADMs can maximize the atomic efficiency, which can increase the reactive sites and reduce the metal consumption, and have received much attentions and shown great potential in industry (Fig. 1). However, due to the limitation of synthesis and characterization method, the recognition of ADMs lags behind their applications.

As early as 1925, the researchers found that the uppermost nickel atoms should be the active sites for catalysis [22]. In 2007, Lee and his co-workers studied the properties of Pd atoms by using extended X-ray absorption fine structure (EXAFS) and aberration corrected-transmission electron microscopy (AC-TEM) technology [23]. The concept of "single-atom (SA) catalysis" was clearly put forward for the first time by Zhang Tao and his co-workers in 2011 [24]. Since then, the ADMs have witnessed rapid development and become the frontier research of catalysis. As the metal size decreases, the quantum size effect has greatly changed the intrinsic properties of materials (Fig. 2) [25]. The ADMs can not only improve the metal utilization but also change the traditional research method. The traditional concepts including the metal dispersion, particle size effect, and metal–support interface are not suitable for ADMs. Instead, the electronic structure and the coordination environment of atom sites are the research topics [26–32]. Besides, the advances of synthetic chemistry and characterization method provide opportunities for the precise construction of active centers and put forward the research of catalysis from molecular level to the atomic era.

The isolated metal atoms anchored on the support can be greatly affected by surface properties, and can be adjusted by tailoring the coordination environment. The metal atoms were fixed on the oxides through oxygen coordination. N acts as the anchoring sites for metal atoms on carbon nitride (CN) materials. And S can also stabilize metal site in many cases [33]. The ADMs with unsaturated coordination status could facilitate the intrinsic
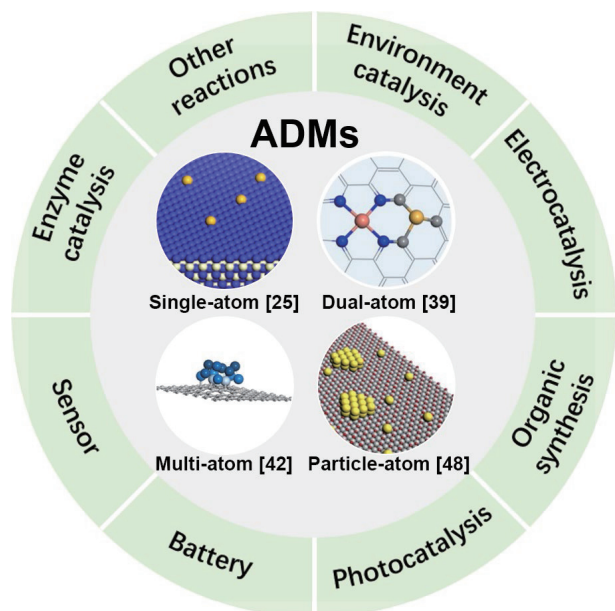
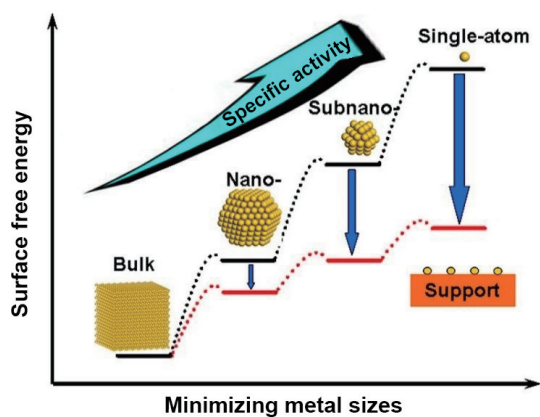**Figure 1** Overview of the topics covered in this review.

Figure 2 Schematic illustration of the surface free energy and specific activity changes as the metal size decreases. Reproduced with permission from Ref. [25], © American Chemical Society 2013.

activity improvement by accelerating the reactant activation [34]. The ADMs with stable coordination structure can always tolerate the harsh reaction conditions as well as maintain the excellent stability [35]. The electronic metal–support interaction can also alter the electronic structure of ADMs and realize the regulation of catalytic performance. With the in-depth study of ADMs, various atomic combination structures have been developed. The concept of "atomically dispersed" is expending from single-atom sites [36] to dual-atom sites [37–41], further to collection of single atoms [42, 43], ensemble sites [44, 45], and cooperation of particles and single atoms [46–48]. Different atomic combinations bring new properties to the active sites [49]. Moreover, the different properties of active centers can provide more possibilities for activating reactants and catalyzing various reactions. The study of ADMs will bring new opportunities for developing ideal catalysts in atomic era.

Previous reviews of ADMs mainly focused on the progress in the design and characterizations of single-atom catalysts. But other atomic combination structures and the summary of reaction progress are simple. Besides, most of works only summarize a single type of reactions such as photocatalysis, electrocatalysis, and a few thermal catalysis reactions. The rapid development of ADMs has greatly expanded their application fields. It reminds us to organize their application areas more comprehensively. In this review, we systematically summarized the application and

progress of ADMs in various fields, including environment catalysis, electrocatalysis, organic synthesis, photocatalysis, battery, sensor, enzyme catalysis, and so on. Finally, we discussed the opportunities and challenges faced by ADMs in various reactions. We hope the comprehensive review can provide instructive advice for the research and application of ADMs.

2 Application of atomically dispersed materials

2.1 Environment catalysis

Environment catalysis is an effective way to eliminate pollutants like CO, NO_x, and hydrocarbons. The pollutant molecules are oxidized into non-toxic and harmless CO_2 and water through catalytic reaction. This technology has multiple advantages such as high efficiency, low energy consumption, and no secondary pollution [50]. The most fundamental requirement is to develop more efficient and stable catalysts. Besides, diverse catalysts should be developed to meet the demand due to the different properties of multiple pollutants. The appropriate catalyst can not only improve the reaction efficiency, but also save costs. We summarized the research progress of different pollutant molecules as follows.

2.1.1 CO oxidation

CO is a kind of toxic gas and has great threat to human health [51]. CO mainly comes from the automobile exhaust emission and fossil fuel combustion. Catalytic CO oxidation has proven to be a successful technology and has great value in industrial application. Besides, CO oxidation also acts as a probe reaction [52, 53]. The relevant achievements have deepened the understanding of interface reactions, and further promoted the development of heterogeneous catalysis. Pd [54–56], Pt [57–60], and Au [61] are commonly used noble metal catalysts. However, their low-temperature activity and high-temperature thermal stability still need to be improved. ADMs have shown unique advantages for CO oxidation. Besides, the development of ADMs brings new opportunities to solve the above problems. Zhang's group prepared the Pt_1/FeO_x catalyst which has shown superior activity in CO oxidation and the turnover frequency (TOF) value was 2–3 times higher than the reference sample [24]. Subsequently, the concept of atomic sites catalysis has attracted more and more attention. The reducible oxides are always used as supports for metal atom loading. Wan et al. prepared the Au-SA/Def-TiO_2 catalyst, in which Au atom was deposed on defective TiO_2 nanosheets (Fig. 3) [62]. The defect site of TiO_2 can stabilize Au atoms as well as form the Ti-Au-Ti structure. It can not only reduce the energy barrier but also weaken the competitive adsorption of Au sites. Cu single-atom catalysts are also effective for CO oxidation [63, 64]. Guo et al. designed the Cu_1/TiO_2 catalyst, in which Cu atoms were trapped by Ti vacancy [63]. The charge transfer between Cu and TiO_2 creates abundant Cu(I) and 2-coordinated O_{lat} sites. The Cu_1–O–Ti structure can distort the TiO_2 lattice and activate the adjacent surface lattice O^{2-}. Detailed studies show that CO oxidation on Cu_1/TiO_2 follows Eley–Rideal route at 80 °C and Mars–van Krevelen route higher than 200 °C.

Since the atomic sites are easy to sinter at higher temperature [65], numerous works and efforts have been made to exploit new synthesis strategy and construct more stable structure of ADMs. The support trapping effect is an effective way to prepare the stable ADMs. For example, Jones et al. used the ceria as support to anchor the Pt atoms. The high temperature treatment during catalyst preparation leads to the mobile PtO_2 to rapidly emit and be finally trapped by ceria through the formation of stable covalent metal oxide bond. The high synthesis temperature also
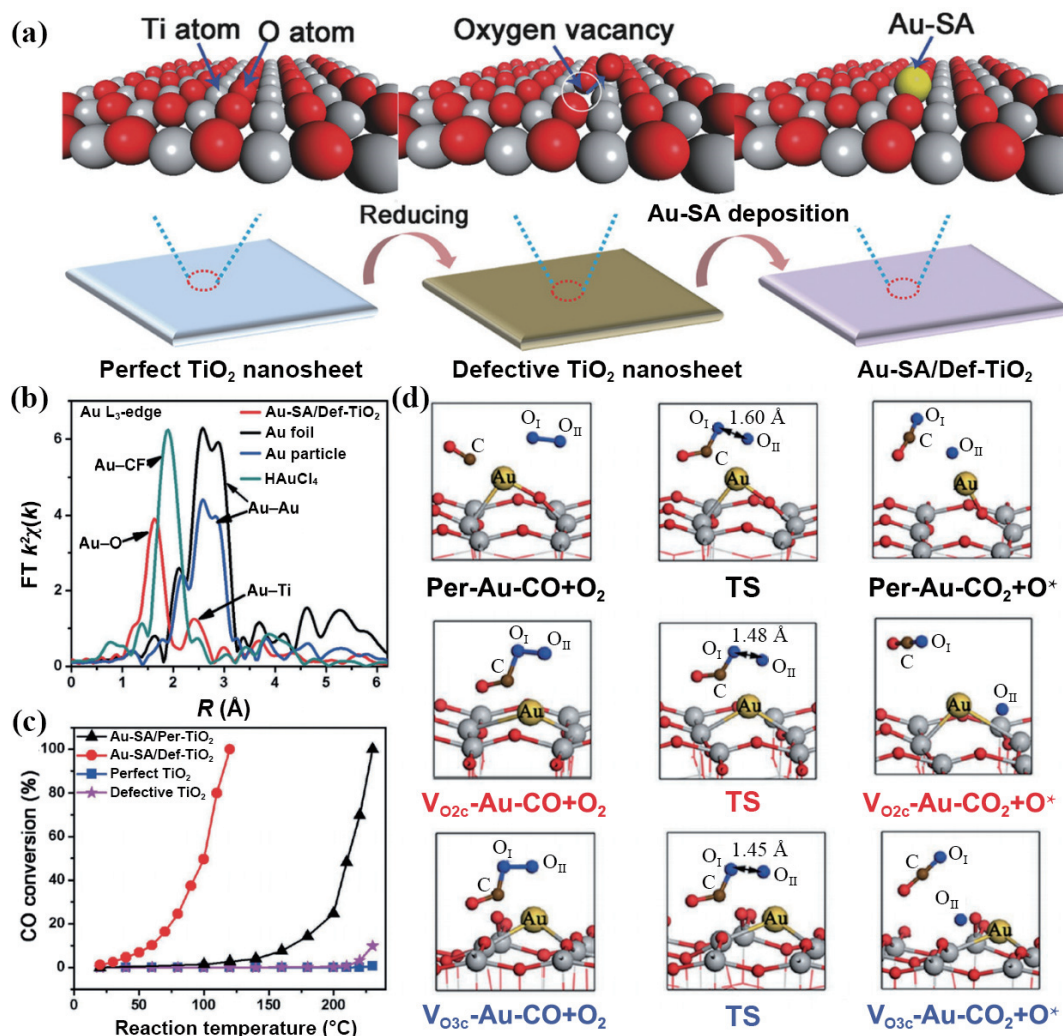
Figure 3 (a) Schematic illustration of catalyst synthesis. (b) Fourier transform (FT)-EXAFS results. (c) Light-off curves for CO oxidation. (d) Simulation of CO oxidation. Reproduced with permission from Ref. [62], © WILEY-VCH Verlag GmbH & Co. KGaA, Weinheim 2018.

ensures the formation of anti-sinter ADMs [66]. However, the stable structure limits their low-temperature activity. Nie et al. activated the surface lattice oxygen of Pt_1/CeO_2 by using a high temperature steam treatment [67]. New active site is generated on CeO_2 near the Pt^{2+} center. The optimal catalyst can achieve excellent low-temperature activity as well as outstanding hydrothermal stability. There will be no significant loss of activity even if the catalyst undergoes harsh reaction conditions. This work makes the ADMs closer to the industrial application. Because the sintering is the key factor to limit their application, strong metal–oxygen interactions can inhibit metal atoms sintering. However, it will also lead to few metal sites available for reactant activation. Besides, the atom sites anchored by oxides are also sintered under high temperature reduction. Recently, Liu and his co-workers designed the defective CeO_x nanoglue islands on SiO_2 and each island hosts one Pt atom averagely [68]. The whole process for catalyst preparation was realized by precisely regulating the pH value, followed by sequential adsorption and deposition of metal ions. Pt can maintain atomic dispersion under both high temperature oxidizing and reducing. Besides, the activated catalyst owns great enhanced CO oxidation activity. Not only the noble metal atoms, atomically dispersed iron hydroxide can also enhance the CO oxidation activity. Lu and his co-workers used the atomic layer deposition (ALD) method to fabricate atomically dispersed $Fe_1(OH)_x$ on Pt particles [69]. The catalysts own excellent activity for selective CO removal, which is about 30 times higher than the traditional Pt on Fe_2O_3 catalysts. The

structure characterization shows that $Fe_1(OH)_x$ clusters anchored on Pt particles and the interfacial sites are the reactive centers to activate CO and O_2. The deposition of $Fe_1(OH)_x$ supplies a new way to construct the highly active catalysts.

Another effective way to construct stable and high-performance catalysts is to regulate the coordination environment of ADMs [70]. For example, Pt atoms are stabilized at CeO_2 surface by forming the Pt_1O_4 symmetric square-planar structure. The overly stable coordination environment makes Pt atoms resistant sintering, as well as reduces the ability to activate reactant molecules [71]. Wang's group developed a thermal-shock technology to reconstruct CeO_2 surface to form an asymmetric Pt_1O_4 structure, and restrict the transport of vapor PtO_2 (Fig. 4). The new coordination structure leads to Pt_1/CeO_2_TS catalysts with high catalytic activity and T_{50} decreased about 140 °C. Moreover, unlike the traditional metallic Pt catalysts with loss activity at high temperature oxidation, the prepared Pt_1/CeO_2_TS can retain the superior activity even at 500 °C. *In situ* diffuse reflectance infrared Fourier transform spectroscopy (DRIFTS) results show that the improved performance can be ascribed to form a partially reduced $Pt_1^{\delta+}$ species during CO oxidation [72]. This finding also inspired us to develop novel methods to synthesize catalysts.

Pd ADMs materials are also suitable for CO oxidation and have shown both similarities and differences with Pt. For example, the atom-trapping effect is also applicable to Pd catalyst. However, unlike Pt, Pd catalysts can be used without reduction activation.

Muravev et al. studied two different Pd/CeO_2 catalysts in CO oxidation and found different dynamic structure evolution [54]. The impregnated Pd atoms tend to reduction and aggregation during CO oxidation. Pd-doped CeO_2 prepared by flame spray pyrolysis still maintains intact in the same process. The isolated Pd^{2+} sites are reactive centers on both two catalysts in low temperature range. Pd doped into CeO_2 can activate the lattice oxygen and promote the oxygen exchange at Pd–O–Ce interface.

2.1.2 NO_x elimination

NO_x is one of the main air pollutants which mainly comes from industry production, vehicle emission, fuel combustion, and so on. The NO_x emission will lead to serious environmental problems including photochemical smog and acid rains. ADMs show good performance in NO_x elimination [73–75]. Wang's group prepared the Rh_1/CeO_2 catalyst by the atom-trapping method [76]. The 0.1 wt.% Rh can achieve high TOF of around 330 h^{-1} and NO can be fully converted at 120 °C. Besides, the low-temperature activity can be further promoted by the presence of water. Zhang et al. deeply studied the reaction mechanism of NO+CO on Rh_1/SiO_2 [77]. The experiment and density functional theory (DFT) results show that CO and NO were adsorbed on Rh atoms and coupled to form the CO_2 and adsorbed N atom. Subsequently, the adsorbed N atom coupled with another CO to form –NCO. The –NCO bound on Rh_1 sites can transfer to SiO_2 to form Si-NCO or couple with NO to form N_2 and CO_2. In another route, the N atom couples with another NO to form N_2O. Finally, N_2O reacts with the adsorbed CO to form CO_2 and N_2. Although noble metal catalysts have excellent performance for NO_x elimination, the high-cost greatly limits their application. Selective catalytic reduction (SCR) technology is the most promising method for NO_x decomposition. Using SCR technology to develop non-noble metal catalysts to replace noble metal catalysts is an effective strategy. Qu et al. designed the Mo_1/Fe_2O_3 catalyst and it has shown high SCR turnover frequency, which is even comparable to the classical V_2O_5/TiO_2 catalyst [78]. The detailed structural characterization shows that the isolated Mo acidic sites and adjacent redox Fe ions composed the dinuclear acid-redox sites. The increase of dinuclear active sites will lead to a higher SCR rate but not change the apparent activation energy.

2.1.3 Three-way catalytic reaction

The engine exhaust gas is mainly composed of CO, NO, C_3H_8, and C_3H_6. Meanwhile, the catalytic reaction is also carried out under harsh conditions. Therefore, it put forward higher requirements for the catalytic activity and stability of the three-way catalysts [79–81]. As for the elimination of complex pollutants, the full dispersion ensemble sites with multiple atomic combination have shown better performance than the isolated sites, since the former with multiple metal centers can provide active sites for various reactant molecules activation. For example, the Pt, Pd, and Rh catalysts with ensemble metal centers have shown excellent activity and durability for automotive applications. CO, C_3H_6, and C_3H_8 can be oxidized at low temperature and NO is also reduced at the same time. The exposed metal centers are metallic ensemble sites instead of isolated atoms. The structure characterizations show that the catalyst can maintain stable before and after the reaction [44]. Zhou et al. prepared the Pt-Pd dual-site single-atom catalyst for three-way catalytic reaction [82]. CeO_2 was used as the support, and Pt and Pd atoms were anchored on CeO_2 by a multi-step heating strategy. The prepared catalysts have shown outstanding TWC performance. Moreover, the ignition temperature of NO can be further decreased by increasing Pt and Pd loading. The DRIFTS results indicate that the neighboring Pt-O-Pd structure acts as the reactive center. CO and NO can be adsorbed separately on Pt and Pd atoms and further promote the NO elimination.
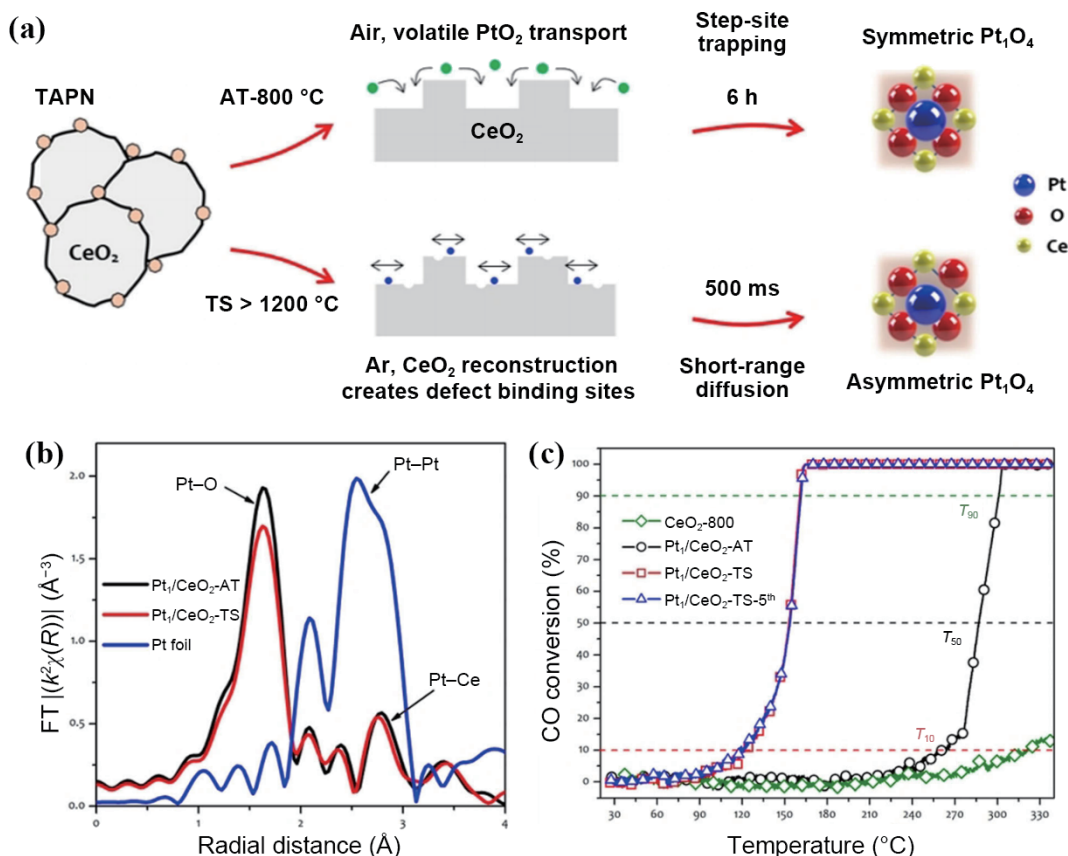

Figure 4 (a) Synthesis different Pt_1/CeO_2 catalysts. (b) FT-EXAFS results. (c) Light-off curves for CO oxidation. Reproduced with permission from Ref. [72], © Wiley-VCH GmbH 2021.

2.1.4 Volatile organic compounds (VOCs) oxidation

VOCs generally refer to organic compounds with boiling point lower than 250 °C under standard atmospheric pressure (101.325 kPa), and are one of the main pollutants in the atmosphere. Most of VOCs can cause secondary pollution, such as ozone pollution and secondary aerogel pollution, which brings serious environmental pollution problems and seriously harms human health [83]. VOCs in the atmosphere mainly come from industrial emissions and vehicle exhaust emissions, while indoor pollution mainly comes from office supplies, decorative materials, and building materials. The main types of VOCs emitted include alkanes, alkynes, olefins, alcohols, ketones, aromatic hydrocarbons, aldehydes, halohydrocarbons, esters, and nitrogen and sulfur compounds. Among them, aromatic hydrocarbons and olefins are highly polluting molecules that need to be solved urgently because they can cause serious environmental problems such as photochemical smog and ozone pollution [50]. The ADMs of Pt, Pd, Au, and Ag have been widely studied and have shown excellent activity for oxygen containing VOCs including formaldehyde, methanol, and acetone. MnO_2 is suitable material for VOCs elimination as well as good support for preparing high performance ADMs [84, 85]. For example, Chen et al. synthesized the α-MnO_2 doped Au catalyst by redox precipitation method [86]. The Cs-corrected high-angle annular dark-field scanning TEM (HAADF-STEM) images indicate that Au atoms were highly dispersed on MnO_2. 0.25% Au/α-MnO_2 can completely remove 500 ppm HCHO at 75 °C. Besides, the catalyst can also eliminate low-concentration HCHO (1 ppm) at ambient temperature. The surface vacancy oxygen, lattice oxygen, as well as charged Au species act as the reactive center. The Mars–van

Krevelen mechanism was also confirmed by the *in situ* DRIFTS results. Hu et al. prepared the Ag_{AOR}-hollandite manganese oxide (HMO) catalyst by anti-Ostwald ripening (AOR) method [87]. The single-atom Ag catalyst with stable structure and controllable electronic state has shown easier reducibility and better catalytic activity.

ADMs also show promising applications in degradation of aromatic hydrocarbons including benzene, toluene, and xylenes. The activation of O_2 and reactant molecules is the prerequisite for catalytic reaction. Platinum has always been used for catalytic oxidation due to its excellent performance [88]. The cooperation between Pt and Fe_2O_3 has been identified for superior activity. Yang et al. designed a three-dimensionally ordered mesoporous iron oxide (meso-Fe_2O_3) by using KIT-6 as template, and further loading Pt atoms to prepare the 0.25Pt_1/meso-Fe_2O_3 catalyst [89]. The optimal catalyst can achieve $T_{50\%}$ and $T_{90\%}$ of benzene oxidation at 186 and 198 °C. The TOF_{Pt} of 0.25Pt_1/meso-Fe_2O_3 is 2.69 s^{-1}, which is much higher than Pt nanoparticles (1.16 s^{-1}) at 160 °C. The catalyst also owns good water resistant, which can be ascribed to the formation of active radicals and carbonates decomposition. Moreover, phenolate, benzoquinone, cyclohexanone, and maleate are the main intermediates during benzene oxidation. Yan et al. reported a new method to prepare thermally stable Pt ADMs (Fig. 5) [90]. Pt single-atom was firstly loaded on Mn_3O_4. The following high-temperature treatment leads to phase transition from Mn_3O_4 to Mn_2O_3. The high-valent Pt^{4+} species can still maintain isolate dispersion state even treatment at 800 °C in humid air for 5 days. The moderate H_2O_2 etching can further promote the catalytic performance as well as thermal stability in CH_4 oxidation. Zhang et al. prepared a
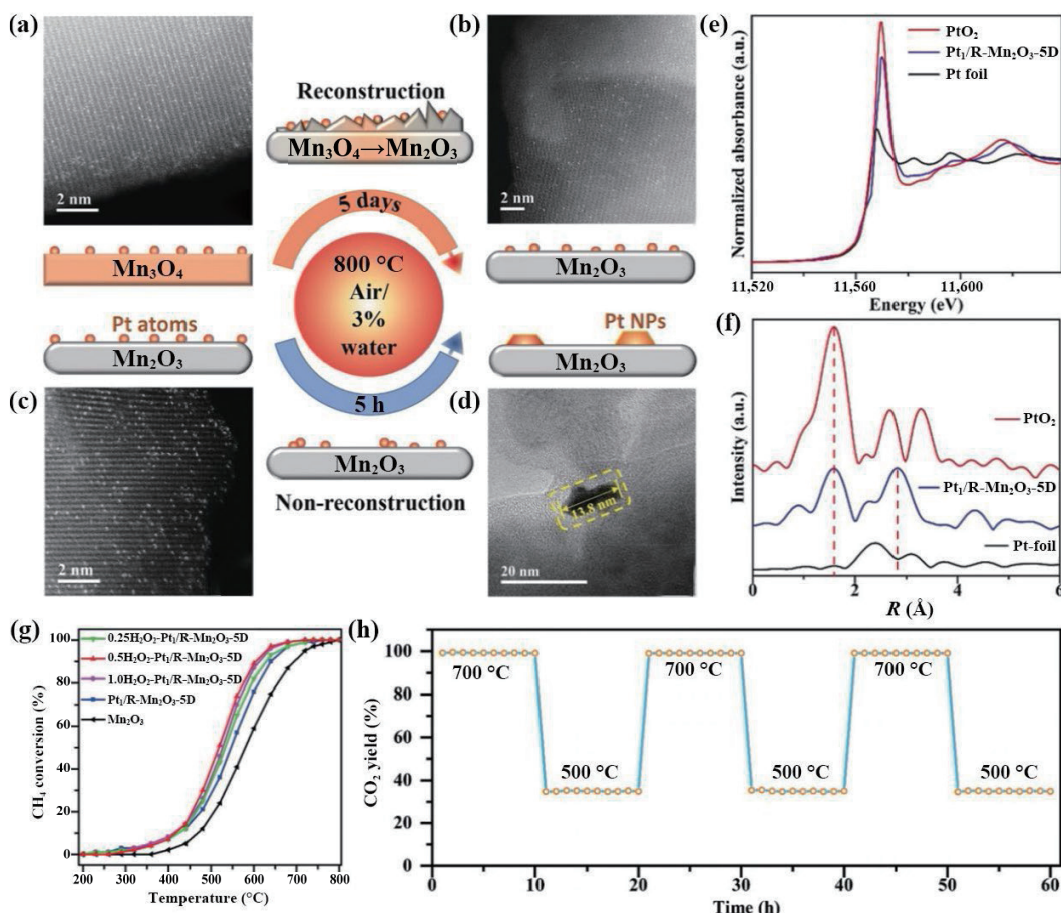

Figure 5 AC-TEM images of (a) Pt_1/Mn_3O_4, (b) Pt_1/R-Mn_2O_3-5D, (c) Pt_1/Mn_2O_3, and (d) Pt_{NP}/Mn_2O_3-5H. (e) X-ray absorption near edge structure (XANES) results. (f) FT-EXAFS results. (g) Light-off curves of CH_4 conversion. (h) Stability test. Reproduced with permission from Ref. [90], © WILEY-VCH Verlag GmbH & Co. KGaA, Weinheim 2020.

Pt/MnO$_2$ catalyst, in which Pt atoms were doped into the defective MnO$_2$ [91]. The catalyst can eliminate 10 ppm toluene at 80 °C, significantly better than the unmodified MnO$_2$. Moreover, Pd can also be used for VOCs elimination. Hou et al. prepared the atomically dispersed tungsten species on Pd nanoparticles [92]. The formed Pd–O–W$_1$ interface structure can promote the water resistance of catalyst in methane combustion. This can be attributed to hydroperoxyl species generation and co-existence of Mars–van Krevelen and Langmuir–Hinshelwood mechanism in the presence of water vapor. The DFT results indicate that electron transfer from W atoms would upshift the d-band center of Pd, which greatly promotes the adsorption and activation of oxygen.

2.2 Application of electrocatalysis

2.2.1 Water splitting

H$_2$ has been recognized as a promising clean energy to replace traditional fossil fuels since its high energy density far exceeds gasoline and coal. Besides, H$_2$ combustion only produces water and has zero carbon emission. It is an ideal green energy and can deal with serious environmental pollution, global warming, energy crisis, and other major threats caused by fossil fuel combustion. Generally, methane steam reforming or coal gasification is used to produce H$_2$ in industry, which will result in large amount of greenhouse gas emissions. Electrocatalytic water splitting to produce H$_2$ is a green and sustainable route with no harmful species formation [93–99]. The water splitting includes hydrogen evolution reaction (HER) process at cathode and oxygen evolution reaction (OER) process at anode.

2.2.1.1 HER

HER occurs at the cathode of electrolytic water dissociation. The reaction substrates are different at different pH values. Generally, hydrogen production follows the two-step continuous reactions (Volmer–Heyrovsky step or Volmer–Tafel step) [29, 100–105]. Platinum has always been an advanced electrocatalyst in HER reaction [106–108]. However, the high cost and scarcity of Pt limit its large-scale application. ADMs can maximize the metal atom utilization. It can effectively reduce the consumption of noble metal while maintaining the number of active sites. Liu et al. designed the onion-like nanospheres of carbon (OLC) for Pt atom loading. Atomically dispersed Pt on Pt$_1$/OLC with only 0.27 wt.% Pt loading has shown high activity in HER, even comparable with commercial 20 wt.% Pt/C. The Pt site with tip-enhanced local electric field is responsible for the high HER activity [109]. For the supported catalysts, the support can regulate the metal properties and plays an important role in the catalytic reaction. Shi et al. prepared different kinds of single Pt atom catalysts by using the site-specific electro-deposition method (Fig. 6) [110]. The Pt atoms were loaded on different types of supports and the structure–activity relationship was studied. They found that the HER activity can be modulated by regulating the electric metal–support interaction and the oxidation states of Pt atom. The correlation between HER activity and average oxidation state of Pt atom as well as the Pt-H/Pt-OH interaction were established. The results show that the hydrogen binding energy decreases with the decrease of Pt oxidation state and finally enhances the acidic HER activity. Pt atoms with optimal oxidation state (ca. +2) own the best alkaline HER activity. More than this, Zhang et al. further studied how the chemical-environment of Pt influenced the HER performance. They prepared a series of Pt ADMs with different axial ligands. The relationship between chemical-environment and HER activity was studied. It follows the sequence as I-Pt < Br-Pt < HO-Pt < F-Pt < Cl-Pt. Besides, Cl-Pt/layered double hydroxide (LDH) has shown the best performance, which can be ascribed to

the high first-electron-affinity of Cl. It can optimize the adsorption of hydrogen and hydroxide, therefore, further promote the alkaline HER [107].

2.2.1.2 OER

OER is another half reaction taking place at anode. Since the OER is a four-electron transfer process, a series of reaction intermediates would be generated. The reaction kinetics of OER is more complex and more difficult to occur compared with the HER. Higher potential is needed to overcome the OER reaction barriers [111, 112]. RuO$_2$ and IrO$_2$ are commonly used commercial catalysts [113–115]. Atomization of noble metals can effectively improve their utilization as well as enhance their mass activity [116]. Cao et al. developed the Ru-N-C ADMs for acidic OER [117]. The mononuclear Ru atom was coordinated with four N atoms to form the porphyrin-like Ru$_1$-N$_4$ structure. The structure will further transform to O-Ru$_1$-N$_4$ after oxygen adsorption and promote the OER activity. Li's group also prepared a Ru/LiCoO$_2$ atomically dispersed catalyst by incorporating Ru atom into LiCoO$_2$ layer (Fig. 7) [118]. The Ru–Co pair sites of the catalyst can enhance the strong electronic coupling between Ru and Co center, thus promote the catalyst electrical conductivity as well as the OER performance. Yao et al. designed a series of Pt-Cu alloys with Ru atoms embedded through acid etching and electrochemical leaching [119]. The volcano relationship between PtCu-alloy lattice constant and OER activity was established. The optimized Ru$_1$-Pt$_3$Cu catalyst shows 220 mV overpotential at 10 mA·cm^{-2} in acidic OER. Moreover, the lifetime is about 10 times longer than the commercial RuO$_2$. The electronic structure of Ru atom was engineered by regulating the compressive strain of Pt shell, which facilitates the oxygen species binding and better resistance to over-oxidation and dissolution. Ir ADMs are also suitable for OER. Jiang et al. prepared the Ir single-atom catalyst on nanoporous (Ni$_{0.74}$Fe$_{0.26}$)$_3$P support by a self-reconstruction method [120]. Isolated Ir atoms were dispersed on oxyhydroxides. The catalyst owned outstanding OER performance and excellent cycling stability, which is comparable to the commercial IrO$_2$ catalyst. The isolated Ir sites are the reactive center and promote the O–O coupling. Although the decomposition of metal into atoms can improve its utilization efficiency, the high cost and scarcity of noble metal have restricted their application. Many efforts have been made to develop non-noble metal catalysts to replace the precious metal. Hu's group prepared a series of double-atom catalysts on N-doped carbon, which were derived from the single-atom precatalysts containing Fe, Co, and Ni. The bimetallic cooperation leads to a higher OER activity of double-atom catalysts compared to the single-atom counterparts [121]. Chen et al. also designed a diatomic site catalyst composed of adjacent Ni and Fe centers [122]. The catalyst shows extraordinary activity and stability for OER. The mechanism study shows that Fe serves as the catalytic center. The orbital coupling of Fe and Ni leads to higher oxidation state of Fe and weakens the binding of intermediate.

2.2.2 Oxygen reduction reaction (ORR)

Fuel cells are promising next-generation energy [123–129]. However, the slow ORR process at cathode is the main obstacle restricting the large-scale application of proton exchange membrane fuel cell (PEMFC) technology. More than this, the ORR catalyst currently used is commercial Pt/C with high Pt loading (higher than 20 wt.%). The key to overcome this obstacle is to reduce the overpotential of ORR to improve the energy conversion efficiency of fuel cells and reduce the cost of catalyst. The development of ADMs can well meet the above requirements. The ORR process involves a multi-step electron transfer. There are
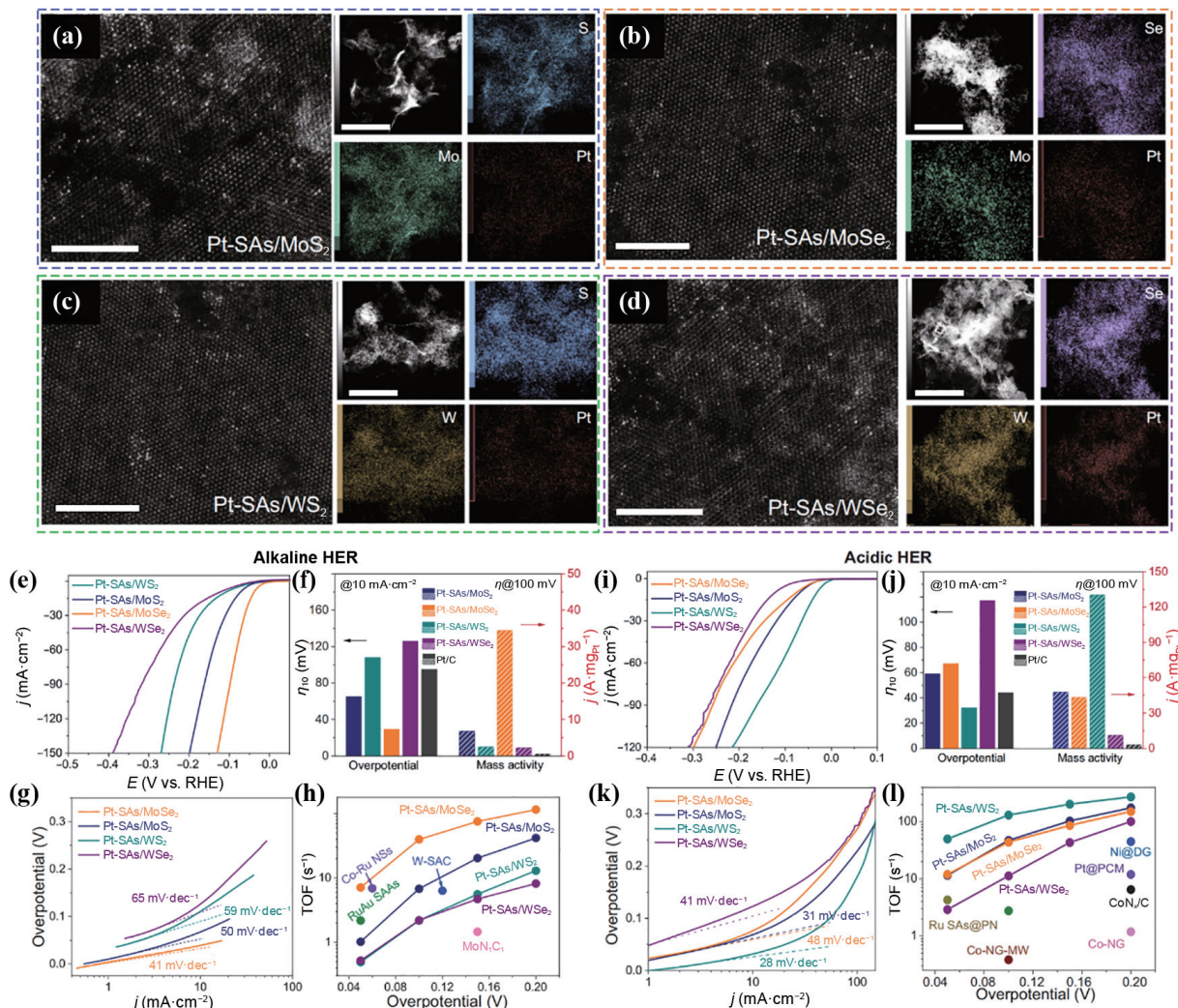
Figure 6 AC-TEM images for (a) Pt-SAs/MoS$_2$, (b) Pt-SAs/MoSe$_2$, (c) Pt-SAs/WS$_2$, and (d) Pt-SAs/WSe$_2$ (scale bars: 5 nm), and elemental mapping (scale bars: 100 nm). (e) and (i) Polarization curves of different samples. (f) and (j) Overpotential and mass activity results of different samples. (g) and (k) Tafel plots. (h) and (l) TOF values. Reproduced with permission from Ref. [110], © Shi, Y. et al. 2021.

two main ways: Oxygen is reduced to water through a direct four electron process; oxygen is first reduced to hydrogen peroxide (or intermediate HO$_2^-$) through a two-electron process, and then reduced to water through a two-electron process. Among them, the direct four-electron process is more efficient than the two-electron process, which makes the battery have better performance and efficiency. The ORR reaction path and catalytic activity are closely related to the intrinsic structure of the catalyst. The analysis of ORR active sites is of great significance for the development of highly efficient catalysts. In recent years, carbon supported Pt atomic catalyst has shown promising application toward ORR. Liu et al. designed a defective carbon to support Pt atoms and achieved high Pt utilization [130]. The prepared Pt$_{1.1}$/BP$_{defect}$ with 1.1 wt.% Pt loading has shown remarkable ORR performance. The structure analysis revealed that each Pt atom was anchored by four carbon atoms in carbon divacancies to form the Pt-C$_4$ structure. Song et al. prepared the Pt single atom catalysts by ALD method [131]. The metal-organic framework (MOF) derived N-doped carbon was used as the support. The Pt catalysts with different sizes can be tailored by changing the ALD exposure time. The 30 s ALD will form Pt single atom and further increasing the deposition time will lead to Pt cluster or nanoparticles formation. The atomically dispersed Pt catalyst shows 6.5 times higher mass activity than Pt nanoparticles. The site density of ADMs can also affect the ORR activity. In addition to the above Pt-carbon catalysts, the combination of Pt and oxides can also contribute to

the highly active catalysts for ORR. Zou's group prepared the Pt–Fe pair sites catalyst [132]. α-Fe$_2$O$_3$ with (012) and (001) crystal planes was selected as the support to load Pt atoms. The different supports show different binding forms with Pt. The strong electronic coupling of Pt–Fe pair on Pt$_1$-Fe/Fe$_2$O$_3$ (012) causes incomplete occupation of orbitals, which accelerates the adsorption and dissociation of O$_2$. The Pt sites also have a good desorption for the intermediate OH* species. The prepared catalysts have shown excellent ORR activity and stability as well as negligible activity attenuation. With the development of fuel cell technology, reducing the cost has become an urgent demand. Replacing the Pt based catalysts by non-noble metal catalyst is an efficient strategy. The researchers developed various non-noble metal ADMs for ORR [133]. For example, Jin et al. prepared a series of Fe-N$_4$ catalysts and regulated the inter-site distance by changing the loading amount of Fe [134]. The results show that as the inter-site distance is less than 1.2 nm, the ORR activity of Fe-N$_4$ catalyst would increase. This can be ascribed to the strong interactions between adjacent Fe-N$_4$ centers, which changes the electronic structure of the reactive center. Moreover, the ORR performance can be further enhanced until the distances of Fe atoms were close to 0.7 nm.

H$_2$O$_2$ is an important disinfectant and oxidant in medical and chemical industry. The traditional production of H$_2$O$_2$ in industry is anthraquinone redox. The impure H$_2$O$_2$ needs further purification and distillation. This process is accompanied by high
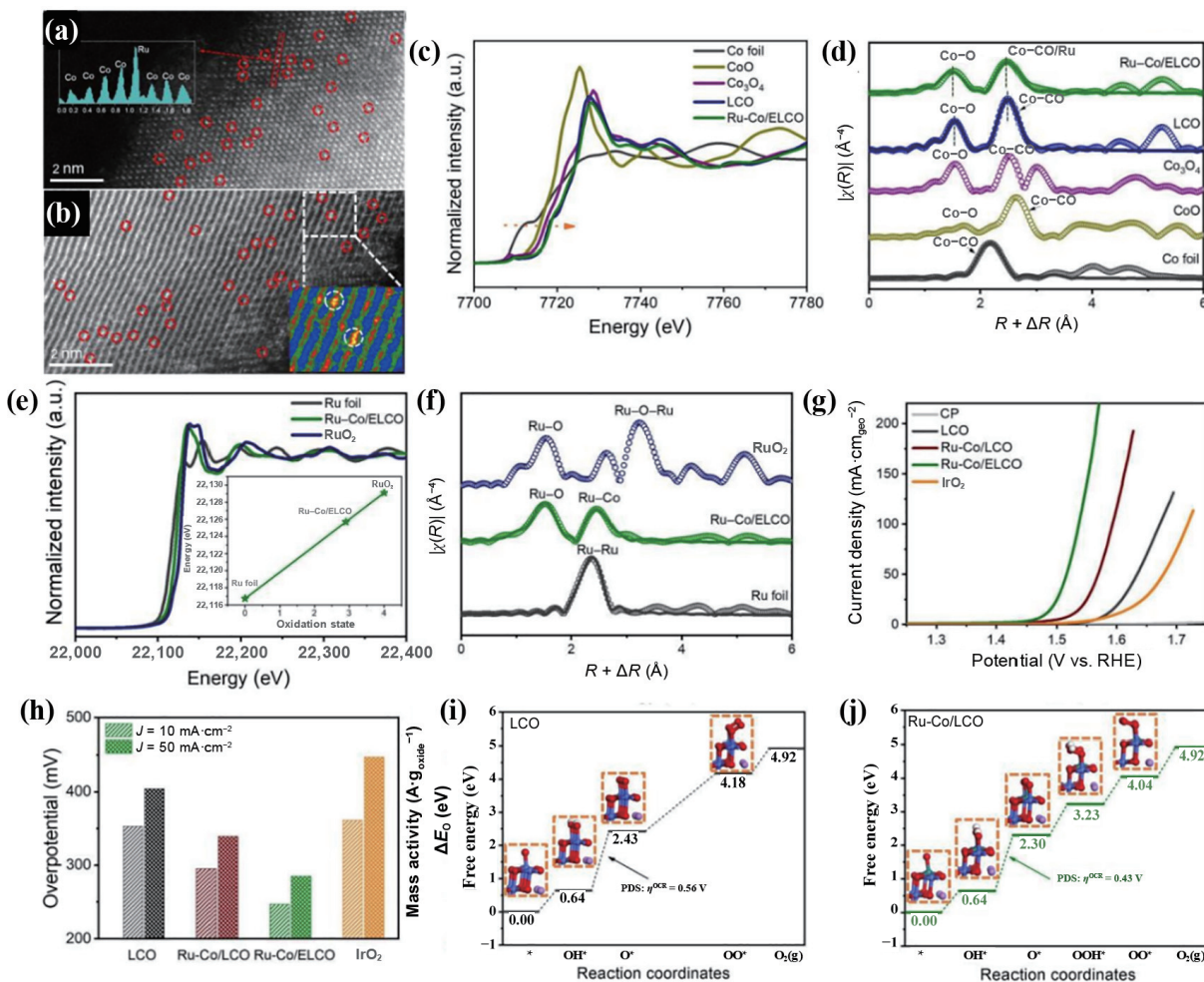
Figure 7 (a) and (b) AC-TEM images. (c) Co K-edge spectra. (d) FT-EXAFS results of Co. (e) Ru K-edge spectra. (f) FT-EXAFS results of Ru. (g) Linear sweep voltammetry (LSV) curves. (h) The overpotential results. The Gibbs free energy for (i) lithium cobalt oxide (LCO) and (j) Ru-Co/LCO. Reproduced with permission from Ref. [118], © Wiley-VCH GmbH 2022.

energy consumption and high pollution. The electrochemical two-electron reduction can generate H_2O_2 at ambient conditions without harmful byproducts [135–137]. The ADMs are promising catalysts in this reaction. For example, Zhang et al. reported a single In atoms on hollow carbon rods for $2e^-$ ORR. The accurate synthesis leads to In atom anchored with N, S in the first coordination and B in the second coordination. The In SAs/NSBC catalyst owns high selectivity (above 95%) for H_2O_2 in both neutral and alkaline solution (Fig. 8) [138]. Jiang et al. developed a highly efficient Fe ADMs for electrocatalysis H_2O_2 production. The H_2O_2 selectivity is above 95% in a wide range of pH values. The DFT results show that Fe-C-O coordination is the reactive center for $2e^-$ ORR for H_2O_2. However, the Fe-C-N prefers to the $4e^-$ way [139].

2.2.3 Electrooxidation of methanol, ethanol, and formic acid

Direct fluid fuel cells use liquid fuel for anodic reaction to convert chemical energy into electrical energy, which has potential to replace traditional fossil energy. Methanol, ethanol, and formic acid are commonly used because of their high energy density and environment-friendly [140–144]. Pt is an excellent electrocatalyst in HER, ORR, methanol oxidation reaction (MOR), and ethanol oxidation reaction (EOR). But, limited by its high cost and scarcity, improving the mass activity of Pt can reduce the consumption of Pt while maintaining the overall activity. Li et al. first prepared PtNi alloy nanowires and then dealloyed the nanowires by a partial electrochemical method to create the Pt nanowires with Ni atom modified. The single Ni atoms can

optimize Pt activity on the surface and enhance the mass activity of HER, MOR, and EOR. Besides, CO will be generated during MOR process and poison the Pt catalyst. It is of great significance to prepare the catalyst against CO poison [145]. Pt_1/RuO_2 catalysts have been reported to show high mass activity in MOR as well as high tolerance for CO poisoning [146]. Poerwoprajitno et al. developed an *in situ* process to construct stable catalyst structure for electrooxidation, in which Pt spreads on Ru branched particles to form Pt atoms dispersed on Ru. The spreading process was confirmed by *in situ* TEM. The formation of stable ADMs structure is driven by strong Pt–Ru bonds. The Pt-on-Ru catalyst can tolerate CO poison and lead to the high mass activity and current density in MOR [147]. Li's group prepared the single Rh atom anchored on N-doped carbon by host–guest strategy [148]. The prepared SA-Rh/CN catalyst has shown ultra-high mass activity as well as high CO tolerance. The mass activity is 67 and 28 times higher than the Pt/C and Pd/C catalysts, respectively. Besides, the catalyst can also maintain stability during the long-term reaction and Rh atoms are sinter resistance.

2.2.4 Carbon dioxide reduction reaction (CO₂RR)

The greenhouse gas CO_2 has triggered serious global climate problem. In recent years, the conversion of CO_2 into high-value hydrocarbon fuels or chemicals has drawn more and more attention [149]. Through energy storage and transformation technology, it can not only reduce the content of CO_2 in the atmosphere, but also convert renewable energy into chemical energy. Besides, the high-value fuels or chemicals formed by CO_2
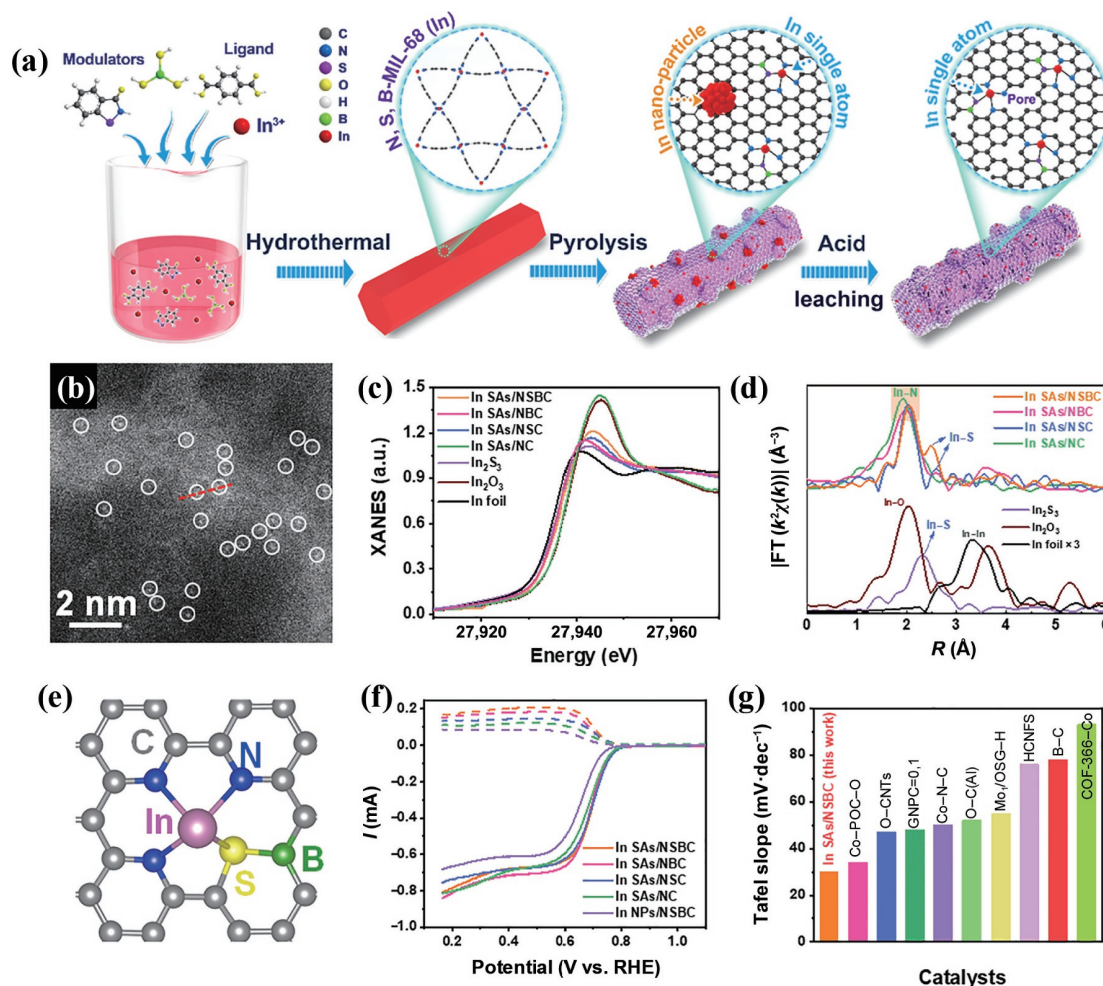
Figure 8 (a) Illustration for catalyst synthesis. (b) AC-TEM image of catalyst. (c) In K-edge XANES results. (d) FT of the k^2-weighted EXAFS results. (e) Structure model of catalyst. (f) Polarization curves. (g) Tafel slope comparison of different samples. Reproduced with permission from Ref. [138], © Wiley-VCH GmbH 2022.

can replace fossil fuels and realize the carbon cycle process. Electrocatalytic CO_2RR into high value chemicals is an effective way to realize this process [150–160]. CO_2RR generally includes the following steps: (1) CO_2 is adsorbed on the surface of catalyst, accepts electrons or protons provided by the electrode, and then the carbon oxygen bond breaks to form related intermediates. (2) Intermediates are rearranged into new reduction products, and then react with protons or electrons in electrolyte or electrode to generate products. Cu has been proved as an effective catalyst for CO_2RR and the products include methane, CO, ethylene, ethanol, and acetate. Chen et al. designed a Cu ADM with N-heterocyclic carbene coordination and embedded into a MOF structure. The catalyst has shown high activity for CO_2 electrocatalysis reduction to CH_4. The CH_4 TOF can achieve 16.3 s^{-1} and the Faradaic efficiency (FE) is as high as 81% for CO_2 to CH_4. The DFT results indicate that the ligated NHC groups increase the electron density of the Cu atoms and promote their adsorption for intermediates [161]. Zhang et al. developed a liquid Ga ADM for CO_2RR. The Ga atoms with P, S coordination have shown high activity for CO_2 reduction to CO and the Faradaic efficiency is about 92%. The outstanding selectivity and stability of CO_2RR can be attributed to the optimal intermediate *COOH adsorption and active sites refresh timely (Fig. 9) [162]. Li's group also found that the nitrogen coordination numbers can be regulated by changing the pyrolyzing temperature of Co/Zn zeolitic imidazolate framework (ZIF). As the temperature rises, more CN species will be released. Different Co-N structures can be obtained as Co-N_2, Co-N_3, and Co-N_4 at 1000, 900, and 800 °C. Co-N_2 owns higher d-band center of −0.81 eV than Co-N_4. The stronger bonding of CO_2^{-} on Co-N_2 sites makes it proper for CO_2 reduction [163].

2.2.5 Nitrogen reduction reaction (NRR)

N_2 is the main component in air and inexhaustible. The electrocatalytic NRR is carried out at ambient pressure and uses H_2O as the proton source. This process is a safe, scalable, low-cost, and environment-friendly NH_3 production strategy [164–169]. N_2 is adsorbed on the catalytic surface and coupled with the multiple electrons and protons. However, the six-electron process makes the reaction more difficult as well as complex side reactions. Since the HER process can be carried out at full pH conditions, it will compete with the NRR process. Gu et al. prepared a W ADM for electrocatalytic NRR [170]. Na_2WO_4 with WO_4 configuration was used as the metal source. The prepared W-NO/NC catalyst has 10 wt.% W loading and W atom was coordinated with N and O. The catalyst has shown both high activity and selectivity for electrochemical NRR to NH_3. The proper binding energy for NRR intermediate should be responsible for the excellent NRR performance. Fe ADMs are also ideal catalysts for NRR. Li et al. prepared the Fe_{SA}-NO-C catalyst, in which N,O-codoped carbon was used for Fe atom loading (Fig. 10) [171]. The structure analysis revealed that Fe atoms are coordinated with four O atoms and two N atoms. The high surface area promotes the mass transfer as well as increases the active sites exposure. Fe_{SA}-NO-C also shows excellent NRR activity and high Faradaic efficiency. The reaction mechanism was also identified by the DFT calculations. The proper adsorption for intermediate, good desorption for NH_x, as well as optimal electron transfer all contribute to the outstanding NRR process. Bimetallic catalyst with atomically dispersed reactive sites has attracted much attention in recent years. Zhang et al. used bacterial cellulose to anchor Fe and Co atoms to prepare Fe-Co dual-atom sites catalyst
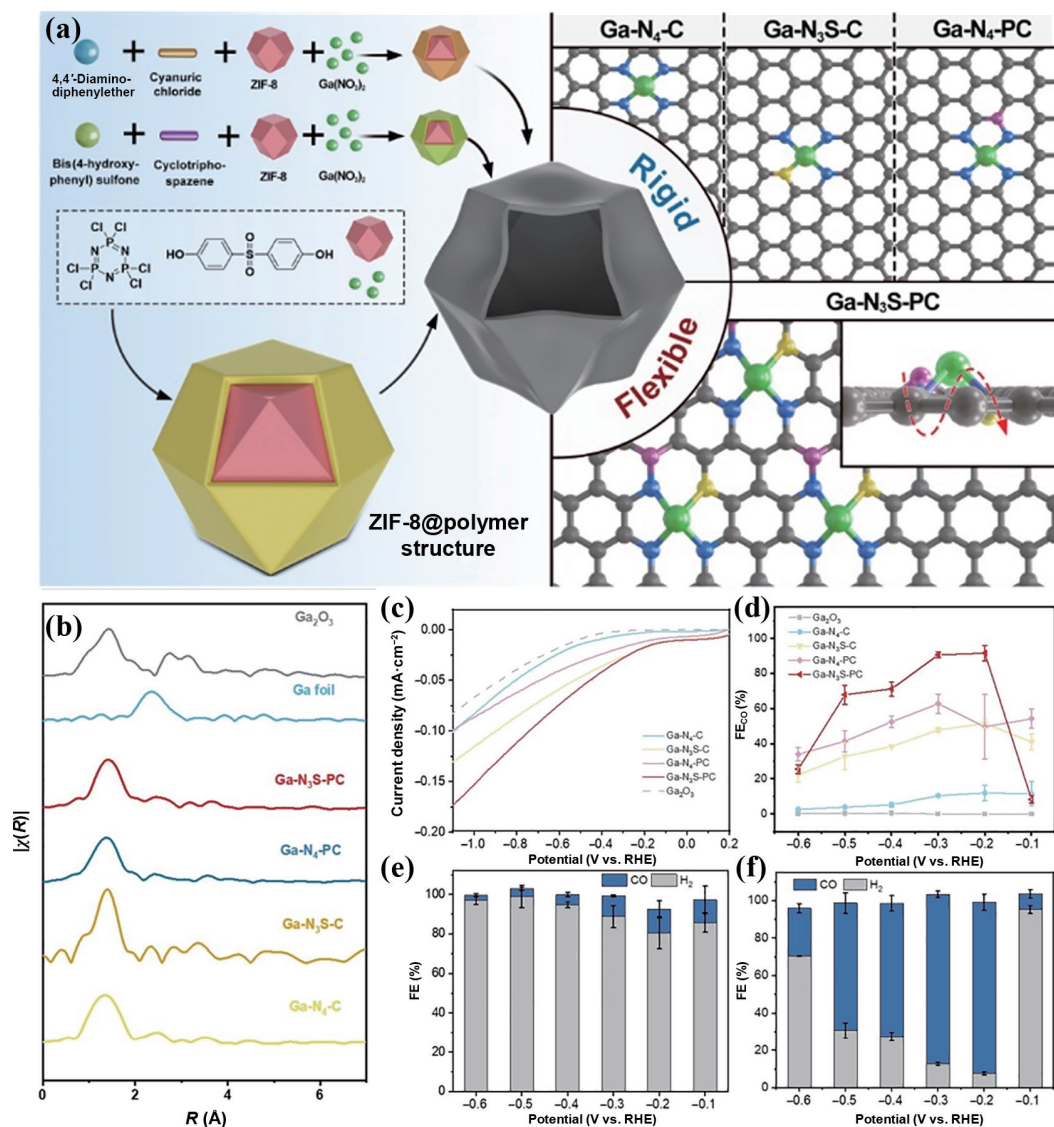
Figure 9 (a) The preparation strategies of different catalysts. (b) *R*-space results for different samples. (c) LSV curves. (d) The CO Faradaic efficiency. (e) CO$_2$RR FE for Ca-N$_4$-C. (f) CO$_2$RR FE for Ca-N$_3$S-PC. Reproduced with permission from Ref. [162], © Wiley-VCH GmbH 2022.

[172]. The rich oxygen groups of bacterial cellulose can adsorb large amount of Fe^{3+} and Co^{2+}. The high density of Fe and Co centers exhibits high activity for NRR.

2.3 Organic synthesis

Using solid catalysts instead of homogeneous catalysts for organic reactions has attracted more and more attention. The solid catalysts have many advantages, such as easy recovery, low cost, and little pollution. Among which, ADMs are famous for their excellent performance in many reactions [173–177]. Their active centers are metal atoms, which own simple and uniform structure, and easy to adjust. The ADMs are promising catalysts for heterogenization of homogeneous reaction. They can not only enhance the catalytic efficiency, but also promote the regioselectivity, chemoselectivity, and stereoselectivity. Besides, they can catalyze many reactions including hydrogenation, oxidation, and C–C coupling reactions.

For example, the synthesized Pd$_1$/TiO$_2$ catalyst by photochemical strategy can be applied to catalyze the hydrogenation of styrene [178]. The easily desorbed activated hydrogen on Pd atoms should be the reason for high catalytic activity. Moreover, the Pt$_1$/FeO$_x$ catalyst shows high activity for hydrogenation of functionalized nitroarenes. The catalytic reaction shows high chemoselectivity and high TOF value [179]. As for the

oxidation reaction, Li's group developed a superior single Co atom catalyst for benzene oxidation to phenol with H$_2$O$_2$. The catalyst showed excellent performance and stability. The formed O=Co=O center promotes the reaction [180]. Hydroformylation as one of the C–C coupling reactions is commonly catalyzed by ADMs. Rh ADMs are suitable catalysts for this reaction. For example, Rh$_1$/CoO has shown better activity than Rh nanoparticles in hydroformylation of propene [181]. Rh$_1$/ZnO owns high selectivity to aldehydes in hydroformylation [182]. Phillip and his co-workers synthesized the pair site Rh–WO$_x$ catalysts for hydroformylation [183]. A bifunctional mechanism was studied based on the experimental kinetics and first principles simulations. The formed Rh–W pair sites have many advantages. It can assist W^{6+} reduction to form the active Rh–W site and promote ethylene transfer from W to Rh. Moreover, the dissociation of H$_2$ at the Rh–WO$_x$ interface creates bridging hydride, which facilitates CO insertion. All above factors work together to make the catalyst with superior activity and selectivity.

2.4 Photocatalysis

In a typical process of photocatalysis, the catalyst was excited to generate electrons and holes under light irradiation, then triggered the redox reaction [184–187]. ADMs always use photoactive materials as support. The metal atoms loaded on photoactive
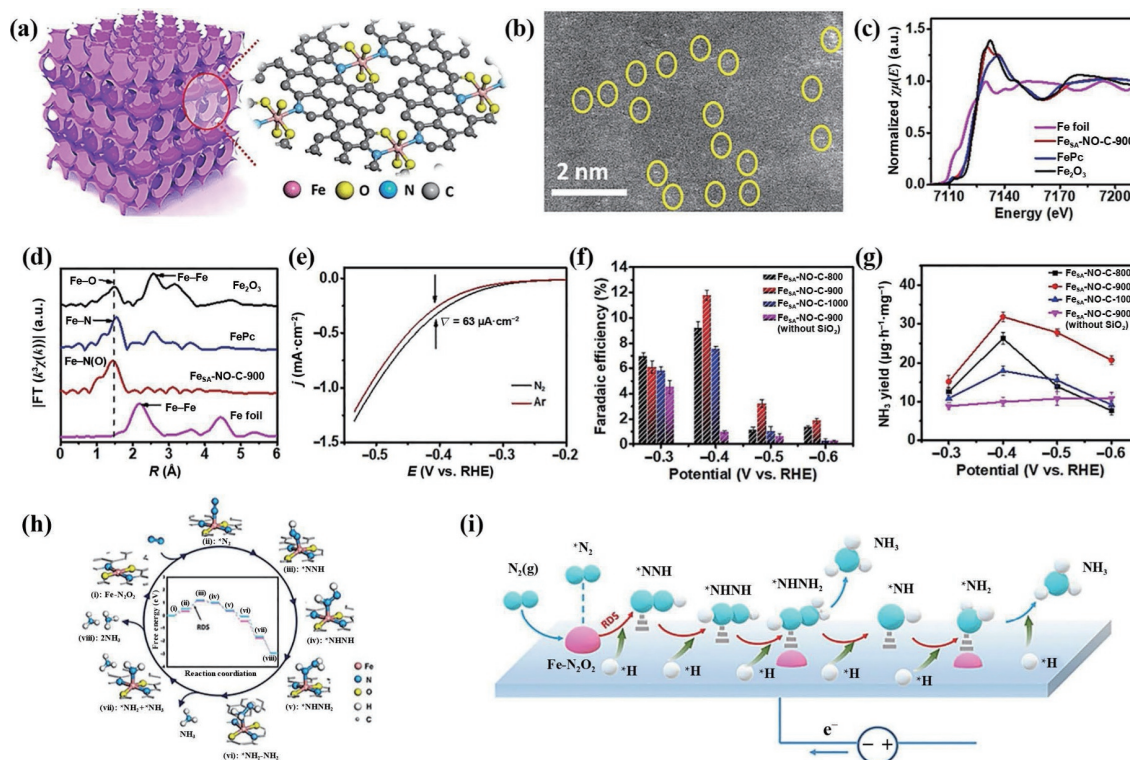
Figure 10 (a) Schematic illustration of catalyst. (b) AC-TEM image. (c) Fe-edge XANES results. (d) FT-EXAFS results. (e) Polarization curves. (f) FE of different samples. (g) NH_3 yield of different samples. (h) The calculated free energy results. (i) Reaction mechanism of N_2 conversion to NH_3. Reproduced with permission from Ref. [171], © Wiley-VCH GmbH 2021.

materials can modify their electronic structure and the energy band structure, and further promote the separation of photogenerated electrons–holes and inhibit their recombination. It can also increase the density of reaction sites for hydrogen production by hydrolysis ionization. In addition, the adsorption and activation of reactants on the photocatalysts can be tailored by adjusting the metal–support interaction. The ADMs have provided new opportunities for the development of photocatalysis [188]. Following examples are listed to demonstrate the wide applications of photocatalysis.

Solar energy is a kind of clean energy with wide sources and sustainable. Solar energy can be converted to hydrogen through photochemical conversion. The photocatalytic water splitting has attracted more and more attention since hydrogen is a valuable energy carrier. However, the low efficiency of photocatalysis has restricted the water splitting process. Great efforts should be paid to develop more efficient photocatalytic system. Xie's groups prepared the Pt single-atom modified C_3N_4 [189]. The tri-s-triazine structure of C_3N_4 can promote the dispersion and anchoring of Pt atoms. Meanwhile, Pt atoms act as cocatalyst and modulate the electron structure of C_3N_4. The optimized Pt-CN catalyst has shown obvious enhancement of photocatalytic hydrogen production. The excessive emission of CO_2 has caused serious greenhouse effect. The photocatalytic CO_2 reduction can convert the harmful CO_2 into valuable chemical products. This approach has become an ideal route for CO_2 elimination [190–192]. Li's group developed the dual-atoms site catalysts of Co and Mn on carbon nitride for photocatalytic CO_2 conversion [193]. The Mn sites accumulate the photogenerated holes for H_2O oxidation. The Co sites activate CO_2 by increasing the bond length and bond angle. The synergistic effect of Mn and Co centers together contributes to high CO yields. The Haber–Bosch process needs a great deal of energy because of the stable N≡N triple bond of N_2. It is also a great challenge to cleavage of N≡N triple bond for photocatalytic nitrogen fixation. Sun et al. designed the

RuSA/TiO_2 photocatalyst for dinitrogen fixation [194]. The defect of TiO_2 can provide the trapping sites for Ru atoms. The photogenerated electrons accumulate on Ru centers and promote the adsorption and activation of N_2. Moreover, the Mo ADM, a non-noble metal catalyst, has also been identified to promote photocatalytic N_2 fixation [195].

The photocatalysis can also be applicated in other areas, including organic synthesis and environmental remediation [196, 197]. The synthesis of organic compounds in industry often needs heating and pressure. This process is accompanied by high cost and environment pollution. The photocatalytic organic synthesis may be a potential route to solve above problems. The photogenerated electrons, holes, and intermediate radical species can be utilized to promote the reaction. The single-atom photocatalysts have shown great potential in this area. For example, the Ag ADMs can be applied to selective dehalogenation under light irradiation [196]. The Fe atoms loaded on MCM-41 can promote the trichloroethylene (TCE) photocatalytic degradation [197].

2.5 Advanced batteries system

The ADMs can maximize the metal utilization and have shown great potential in battery systems [198]. Although great progress has been made, many factors still need to be considered when the ADMs were applied in battery systems. For example, the loading and exposure of metal active sites should be improved, and the intrinsic mechanisms need to be further clarified. The lithium dendrites have negative effect on the lifetime and stability of lithium battery. Multiple methods have been applied to reveal the Li nucleation mechanism. Transition metal atoms (Fe, Co, and Ni) can be used for lithium metal anode to regulate Li nucleation. The metal atom sites and coordination N atoms can tailor the local structure and improve the adsorption for Li. The strong binding of Li atoms and substrate can inhibit Li nucleation. The metal atom sites can act as lithiophilic centers. Besides, the doping

of metal atom sites can improve the matrix stability as well as enhance the lithium battery cycle life [199, 200].

Lithium-sulfur (Li-S) battery is composed of lithium anode and sulfur cathode. It has many potential advantages including high theoretical capacity, low cost, and more safety. Lithium-sulfur battery has been expected to replace lithium-ion battery. The ADMs can play a role in this field. For example, the Co-N/G bifunction catalyst can be used to decorate the cathodes of Li-S battery [201]. The Co-N-C structure acts as the active center to boost the reduction and oxidation of polysulfides. The separator can also be decorated by ADMs. Zhang et al. prepared the Ni@NG catalyst by *in situ* pyrolysis method. The highly oxidized Ni with unique Ni-N$_4$ structure limits the LiPS dissolution. The Ni-N$_4$ structure can maintain stability after long charge/discharge cycles (Fig. 11) [202]. Moreover, The ADMs can be applied in sodium battery and sodium-sulfur battery. The Zn and Co atomically dispersed catalysts all show great potential in the above fields [203, 204].

2.6 Sensor

The ADMs have shown good performance in gas sensors. The atom-sites would promote the surface oxygen species formation through spillover effect. Besides, the oxygen vacancies are more easily formed due to the promotion effect of isolated atom sites. The abundant oxygen vacancies can greatly improve the sensor performance. The Pt, Pd, Au, and Ag all have shown good performance in gas sensor. Metal oxides are commonl support for anchoring metal atoms [205]. Li's group prepared one-dimensional (1D) Fe$_2$O$_3$ particles supported isolated single atom sites (ISAS) Pt material for gas sensor. By turning the oxidation state and coordination structure of Pt atoms, the optimal Pt$_1$-Fe$_2$O$_3$-ox can achieve better ethanol gas sensor than the Pt particle and bare Fe$_2$O$_3$ support [206]. Moreover, the Co$_3$O$_4$ nanoparticle film with Pd atom modified also shows enhanced hydrogen

sensing performance [207]. Xue et al. prepared the Au$_1$-ZnO nanomaterial which has shown superior NO$_2$ sensing response (Fig. 12) [208]. The ZnO structure can be precisely controlled to form ladder-like morphology. Besides, the abundant unsaturated step defects of ZnO can act as anchor sites for Au atom. The carbon materials are also suitable support to regulate the properties of metal center. Many carbon materials can adjust the coordination environment of the metal centers and improve the intrinsic performance. For example, the transition metal dichalcogenides (TMDs), graphene, and MXenes were used to prepare the ADMs for gas sensing [209–212]. Mao's group designed a Ni atom catalyst for electrochemical NO oxidation [213]. The Ni atoms were anchored on the N-doped hollow carbon spheres. The catalyst owns lower Gibbs free energy for NO activation as compared to the common Ni materials. More than this, the Ni catalyst also shows high biocompatibility.

2.7 Atomically dispersed enzyme catalysis

Nanozyme has attracted more attentions since it can break through the limitation of high cost, low stability, and difficult storage as compared to the natural enzymes. However, the low activity and slow kinetics have restricted their further application. ADMs can mimic the tradition enzymes at atom level due to the well-defined electronic and geometric structures [214–218]. Li's group designed the FeN$_3$P-SAzyme catalyst, in which the coordination structure of Fe atom can be precisely adjusted. The rich doped N and P atoms can improve the catalytic activity. P atoms act as the electron donors and Fe single sites with less positive charge. All these factors work together to decrease the barriers of surface O formation and accelerate the reaction kinetics. The FeN$_3$P-SAzyme with three-dimensional (3D) porous carbon structure can mimic the enzymes with 3D amino acid structure and facilitate the exchange and transfer of substates [214]. Zhu et al. also prepared the PEGylated manganese-based
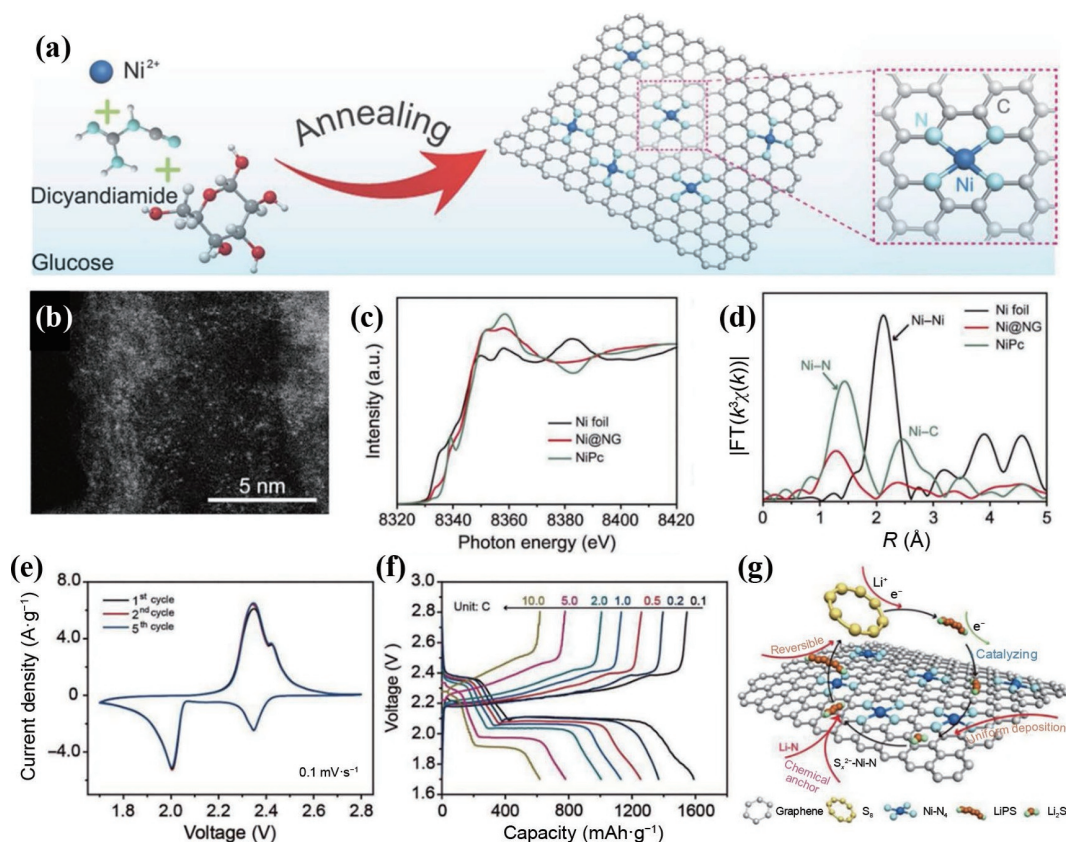

Figure 11 (a) Schematic illustration for catalyst preparation. (b) AC-TEM images. (c) XANES results. (d) FT-EXAFS results. (e) Cyclic voltammetry (CV) curves. (f) Charge/discharge curves of Li-S battery. (g) The proposed reaction mechanism. Reproduced with permission from Ref. [202], © WILEY-VCH Verlag GmbH & Co. KGaA, Weinheim 2019.
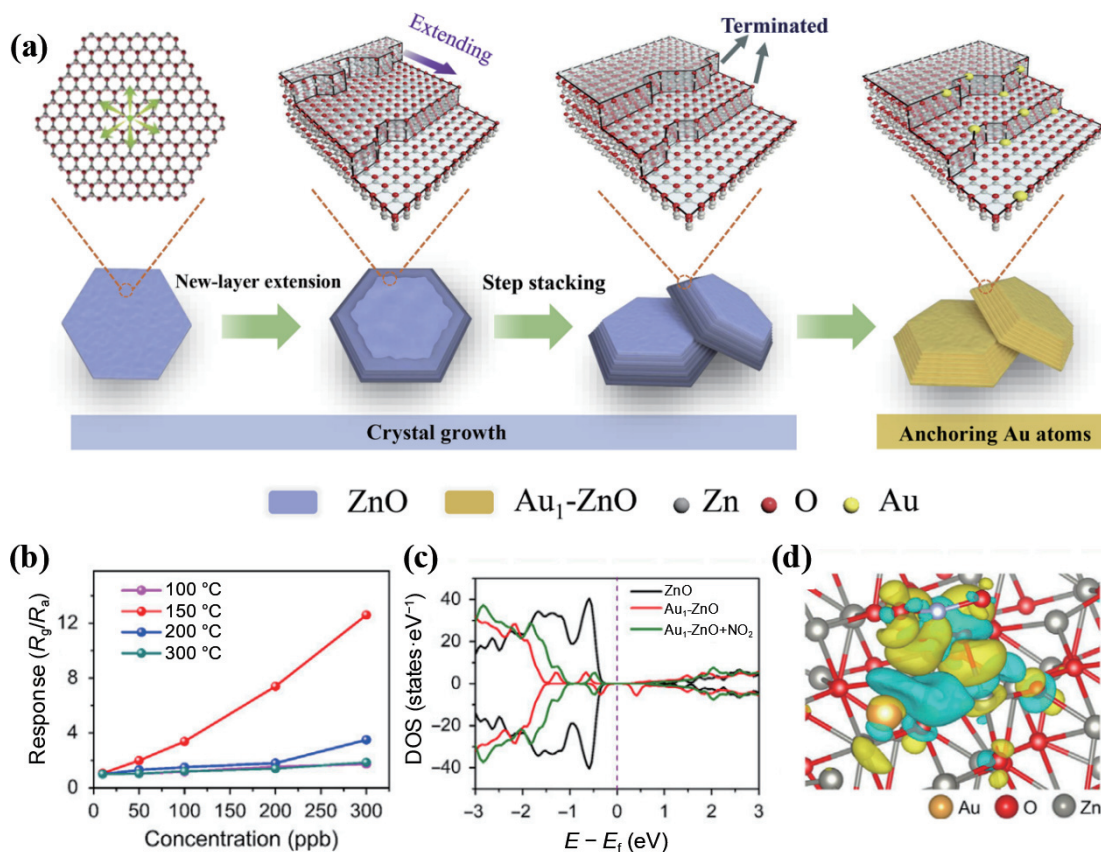
Figure 12 (a) Schematic illustration of layered ZnO anchoring Au atoms with step sites. (b) Response to different concentrations NO_2 at various temperatures. (c) The calculated density of states (DOS) results of different samples. (d) Charge density difference. Reproduced with permission from Ref. [208], © Elsevier Inc. 2020.

single-atom enzyme (Mn/PSAE) for tumor treatment, in which Mn was coordinated with nitrogen atoms in hollow ZIF-8. The catalyst has shown remarkable Fenton reactivity. The reactive oxygen species (ROS) generated in catalytic reaction can kill tumor cells. Besides, the activity of single atom enzyme is significantly higher than the conventional MnO_2 [217]. Guo's group designed a boron-doped Fe-N-C single-atom nanozyme which owns remarkably enhanced activity and selectivity for mimicking nature peroxidase [215]. The studies show that boron-doping can induce electrons rearrangement and lead to a positive charge Fe center. The FeBNC owns lower energy barrier for hydroxyl radical formation and promotes the peroxidase-like activity.

2.8 Other reactions

2.8.1 Water gas shift (WGS) reaction

WGS reaction has attracted extensive attention and been widely studied since it can eliminate trace CO in proton exchange membrane fuel cell and avoid Pt electrode from being poisoned. Au and Pt are commonly used catalysts for WGS [219, 220]. The oxide supported noble-metal catalysts have shown excellent low-temperature activity as well as good stability. In recent years, ADMs have shown great potential in WGS reaction. The development of ADMs brings new opportunities in this field. For example, Flytzani-Stephanopoulos and co-workers prepared the Pt atom catalysts on various supports including L-zeolites, TiO_2, and MCM-41. The atomically dispersed Pt sites were stabilized by sodium through O ligands. Pt-O(OH)$_x$- acts as the reactive center and the support is indirect. Moreover, they also prepared the Au ADMs for low-temperature WGS. The isolated Au-(OH)$_x$ species on TiO_2 support also show good performance [219]. Zhang's group synthesized the Ir_1/FeO_x catalyst which has shown 1 order higher activity than the clusters or particles catalysts. The

reducibility of FeO_x was enhanced by Ir atoms loading and led to the increase in catalytic activity [221].

2.8.2 Acetylene semi-hydrogenation

Ethylene is an important chemical raw material, which is mainly obtained by steam cracking of naphtha in industry. The production of ethylene always contains small amount of acetylene. Acetylene will poison the ethylene polymerization catalyst, and even a small amount of acetylene will lead to deactivation of the catalyst. Therefore, it is necessary to remove acetylene from the outlet gas. The acetylene hydrogenation reaction was commonly used to remove impurity acetylene in industry because it is not only highly efficient, but can also avoid ethylene loss [222–224]. The Pd-based catalyst was always used for acetylene hydrogenation reaction [225–227]. In recent years, the Pd ADMs have shown outstanding performance in this reaction. Gao et al. prepared the Pd/Fe_2O_3 catalyst, in which Pd atoms were loaded on α-Fe_2O_3 (012) (Fig. 13). The Pd–Fe pair sites can promote the adsorption and dissociation of H_2. Pd single atoms were favorable to C=C intermediate desorption. The prepared catalyst has shown high activity and selectivity for alkyne hydrogenation [228].

3   Summary and perspective

ADMs are the hotspot in catalysis due to their high metal utilization and potential economic advantages in industry. The adjustment of coordination environment and electronic structure provides more opportunities for the ADMs development. In this review, we traced the origin and development of ADMs, and discussed the key factors affecting the ADMs performance. Furthermore, we summarized the recent progress of ADMs in various applications including environment catalysis, electrocatalysis, organic synthesis, photocatalysis, battery, sensor,
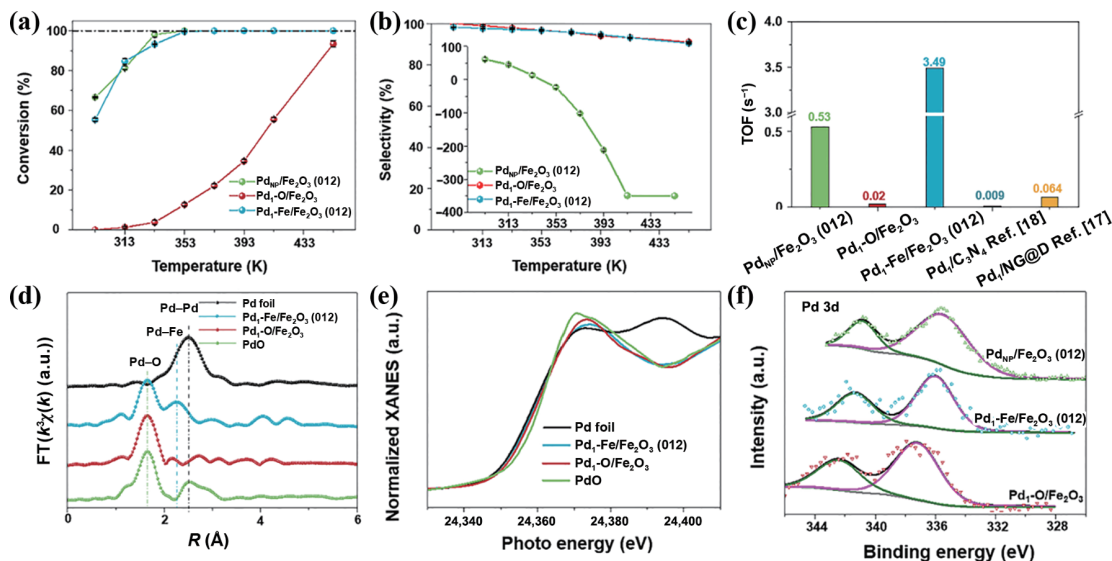
Figure 13 (a) Conversion curves on different samples. (b) The selectivity results of different samples. (c) TOF values of different samples at 313 K. (d) FT-EXAFS results. (e) XANES results. (f) Pd 3d X-ray photoelectron spectroscopy (XPS) results of different samples. Reproduced with permission from Ref. [228], © American Chemical Society 2021.

enzyme catalysis, and so on. With the deepening of research, new problems are constantly discovered and solved. The joint efforts of every researcher have made this field continue to flourish. As many challenges still exist, new efforts are further needed to be paid in following aspects:

(1) Regulate the electronic structure and coordination environment of ADMs. The metal sites are reactive centers for reactants activation, and their properties depend on the electronic structure and coordination environment. Increasing the coordination unsaturated metal sites and regulating the ligand atoms can effectively modulate the metal properties.

(2) Balance the activity and stability of ADMs. The metal atoms are easy to sinter into large particles due to the Oswald ripening. Stabilizing the metal atoms by bonding can effectively improve the stability but reduce the activity for reactants activation. How to improve the low-temperature activity of ADMs in exhaust oxidation while maintaining the long-time stability and high temperature tolerance will be of great significance.

(3) Identification of active sites accurately in actual reactions. The accurate understanding of the reaction center can provide us favorable guidance for rational design new catalysts. The catalytic reaction is a complex process which involves multiple electrons and substances exchange. The adsorption of reactants and intermediates on reactive sites will change its original properties. Thus, it will further increase the complexity of the reaction pathways.

(4) Dynamic evolution of ADMs during catalytic reaction. The atom sites will undergo dynamic structural evolution during catalytic reaction. For example, the reductive molecules will cause metal atoms to be sintered at high temperature reaction. The structure of catalysts changes under the action of electrocatalysis and forms new catalytic structure.

(5) Synergism of dual-atomic sites, multi-atomic sites, or particle-atomic aggregates in catalytic reactions. Generally, the isolated reactive center can only activate a single species. As for complex catalytic reactions involving multiple reactants and processes, the synergy of multiple active sites is needed to enhance the catalytic efficiency. In recent years, the dual-atomic sites, multi-atomic sites, or particle-atomic aggregates have been identified to own advantages in many fields. However, the detailed process and the reaction mechanism still need to be clarified since multiple reactions will cause many side effects.

References

[1] Li, Z.; Ji, S. F.; Liu, Y. W.; Cao, X.; Tian, S. B.; Chen, Y. J.; Niu, Z. Q.; Li, Y. D. Well-defined materials for heterogeneous catalysis: From nanoparticles to isolated single-atom sites. *Chem. Rev.* **2020**, *120*, 623–682.

[2] Smil, V. Detonator of the population explosion. *Nature* **1999**, *400*, 415–415.

[3] Busico, V.; Cipullo, R.; Mingione, A.; Rongo, L. Accelerating the research approach to Ziegler–Natta catalysts. *Ind. Eng. Chem. Res.* **2016**, *55*, 2686–2695.

[4] Huang, C. Y.; Shan, W. P.; Lian, Z. H.; Zhang, Y.; He, H. Recent advances in three-way catalysts of natural gas vehicles. *Catal. Sci. Technol.* **2020**, *10*, 6407–6419.

[5] Kaiser, S. K.; Chen, Z. P.; Akl, D. F.; Mitchell, S.; Pérez-Ramírez, J. Single-atom catalysts across the periodic table. *Chem. Rev.* **2020**, *120*, 11703–11809.

[6] Gan, T.; Chu, X. F.; Qi, H.; Zhang, W. X.; Zou, Y. C.; Yan, W. F.; Liu, G. Pt/Al$_2$O$_3$ with ultralow Pt-loading catalyze toluene oxidation: Promotional synergistic effect of Pt nanoparticles and Al$_2$O$_3$ support. *Appl. Catal. B: Environ.* **2019**, *257*, 117943.

[7] Behrens, M.; Studt, F.; Kasatkin, I.; Kühl, S.; Hävecker, M.; Abild-Pedersen, F.; Zander, S.; Girgsdies, F.; Kurr, P.; Kniep, B. L. et al. The active site of methanol synthesis over Cu/ZnO/Al$_2$O$_3$ industrial catalysts. *Science* **2012**, *336*, 893–897.

[8] Li, D. D.; Xu, F.; Tang, X.; Dai, S.; Pu, T. C.; Liu, X. L.; Tian, P. F.; Xuan, F. Z.; Xu, Z.; Wachs, I. E. et al. Induced activation of the commercial Cu/ZnO/Al$_2$O$_3$ catalyst for the steam reforming of methanol. *Nat. Catal.* **2022**, *5*, 99–108.

[9] Ding, K. L.; Cullen, D. A.; Zhang, L. B.; Cao, Z.; Roy, A. D.; Ivanov, I. N.; Cao, D. M. A general synthesis approach for supported bimetallic nanoparticles via surface inorganometallic chemistry. *Science* **2018**, *362*, 560–564.

[10] Chen, G. W.; Fang, L. Z.; Li, T.; Xiang, Y. Z. Ultralow-loading Pt/Zn hybrid cluster in zeolite HZSM-5 for efficient dehydroaromatization. *J. Am. Chem. Soc.* **2022**, *144*, 11831–11839.

[11] Zhang, Q.; Gao, S. Q.; Yu, J. H. Metal sites in zeolites: Synthesis, characterization, and catalysis. *Chem. Rev.*, in press, https://doi.org/10.1021/acs.chemrev.2c00315.

[12] Hu, Z. P.; Qin, G. Q.; Han, J. F.; Zhang, W. N.; Wang, N.; Zheng, Y. J.; Jiang, Q. K.; Ji, T.; Yuan, Z. Y.; Xiao, J. P. et al. Atomic insight into the local structure and microenvironment of isolated Co-motifs in MFI zeolite frameworks for propane dehydrogenation. *J. Am. Chem. Soc.* **2022**, *144*, 12127–12137.

[13] Cui, T. T.; Ma, L. N.; Wang, S. B.; Ye, C. L.; Liang, X.; Zhang, Z. D.; Meng, G.; Zheng, L. R.; Hu, H. S.; Zhang, J. W. et al. Atomically dispersed Pt-N₃C₁ sites enabling efficient and selective electrocatalytic C–C bond cleavage in lignin models under ambient conditions. *J. Am. Chem. Soc.* **2021**, *143*, 9429–9439.

[14] Jiao, L.; Zhu, J. T.; Zhang, Y.; Yang, W. J.; Zhou, S. Y.; Li, A. W.; Xie, C. F.; Zheng, X. S.; Zhou, W.; Yu, S. H. et al. Non-bonding interaction of neighboring Fe and Ni single-atom pairs on MOF-derived N-doped carbon for enhanced CO_2 electroreduction. *J. Am. Chem. Soc.* **2021**, *143*, 19417–19424.

[15] Zhang, W. J.; Jing, P.; Du, J.; Wu, S. J.; Yan, W. F.; Liu, G. Interfacial-interaction-induced fabrication of biomass-derived porous carbon with enhanced intrinsic active sites. *Chin. J. Catal.* **2022**, *43*, 2231–2239.

[16] Zhou, A. W.; Guo, R. M.; Zhou, J.; Dou, Y. B.; Chen, Y.; Li, J. R. Pd@ZIF-67 derived recyclable Pd-based catalysts with hierarchical pores for high-performance heck reaction. *ACS Sustainable Chem. Eng.* **2018**, *6*, 2103–2111.

[17] Xiong, Y.; Sun, W. M.; Han, Y. H.; Xin, P. Y.; Zheng, X. S.; Yan, W. S.; Dong, J. C.; Zhang, J.; Wang, D. S.; Li, Y. D. Cobalt single atom site catalysts with ultrahigh metal loading for enhanced aerobic oxidation of ethylbenzene. *Nano Res.* **2021**, *14*, 2418–2423.

[18] Tian, S. B.; Hu, M.; Xu, Q.; Gong, W. B.; Chen, W. X.; Yang, J. R.; Zhu, Y. Q.; Chen, C.; He, J.; Liu, Q. et al. Single-atom Fe with Fe₁N₃ structure showing superior performances for both hydrogenation and transfer hydrogenation of nitrobenzene. *Sci. China Mater.* **2020**, *64*, 642–650.

[19] Zhang, Z. D.; Zhou, M.; Chen, Y. J.; Liu, S. J.; Wang, H. F.; Zhang, J.; Ji, S. F.; Wang, D. S.; Li, Y. D. Pd single-atom monolithic catalyst: Functional 3D structure and unique chemical selectivity in hydrogenation reaction. *Sci. China Mater.* **2021**, *64*, 1919–1929.

[20] Wang, B. Q.; Cheng, C.; Jin, M. M.; He, J.; Zhang, H.; Ren, W.; Li, J.; Wang, D. S.; Li, Y. D. A site distance effect induced by reactant molecule matchup in single-atom catalysts for Fenton-like reactions. *Angew. Chem., Int. Ed.* **2022**, *61*, e202207268.

[21] Liu, Z. H.; Du, Y.; Zhang, P. F.; Zhuang, Z. C.; Wang, D. S. Bringing catalytic order out of chaos with nitrogen-doped ordered mesoporous carbon. *Matter* **2021**, *4*, 3161–3194.

[22] Taylor, H. S. A theory of the catalytic surface. *Proc. Roy. Soc. A Mathemat. Phys. Eng. Sci.* **1925**, *108*, 105–111.

[23] Hackett, S. F. J.; Brydson, R. M.; Gass, M. H.; Harvey, I.; Newman, A. D.; Wilson, K.; Lee, A. F. High-activity, single-site mesoporous Pd/Al₂O₃ catalysts for selective aerobic oxidation of allylic alcohols. *Angew. Chem., Int. Ed.* **2007**, *46*, 8593–8596.

[24] Qiao, B. T.; Wang, A. Q.; Yang, X. F.; Allard, L. F.; Jiang, Z.; Cui, Y. T.; Liu, J. Y.; Li, J.; Zhang, T. Single-atom catalysis of CO oxidation using Pt₁/FeO$_x$. *Nat. Chem.* **2011**, *3*, 634–641.

[25] Yang, X. F.; Wang, A. Q.; Qiao, B. T.; Li, J.; Liu, J. Y.; Zhang, T. Single-atom catalysts: A new frontier in heterogeneous catalysis. *Acc. Chem. Res.* **2013**, *46*, 1740–1748.

[26] Zhang, T. Single-atom catalysis: Far beyond the matter of metal dispersion. *Nano Lett.* **2021**, *21*, 9835–9837.

[27] Han, L. L.; Cheng, H.; Liu, W.; Li, H. Q.; Ou, P. F.; Lin, R. Q.; Wang, H. T.; Pao, C. W.; Head, A. R.; Wang, C. H. et al. A single-atom library for guided monometallic and concentration-complex multimetallic designs. *Nat. Mater.* **2022**, *21*, 681–688.

[28] Li, R. Z.; Wang, D. S. Understanding the structure–performance relationship of active sites at atomic scale. *Nano Res.* **2022**, *15*, 6888–6923.

[29] Li, W. H.; Yang, J. R.; Wang, D. S. Long-range interactions in diatomic catalysts boosting electrocatalysis. *Angew. Chem., Int. Ed.* **2022**, *61*, e202213318.

[30] Yang, J. R.; Li, W. H.; Xu, K. N.; Tan, S. D.; Wang, D. S.; Li, Y. D. Regulating the tip effect on single-atom and cluster catalysts: Forming reversible oxygen species with high efficiency in chlorine evolution reaction. *Angew. Chem., Int. Ed.* **2022**, *61*, e202200366.

[31] Gao, Y.; Liu, B. Z.; Wang, D. S. Microenvironment engineering of single/dual-atom catalysts for electrocatalytic application. *Adv. Mater.*, in press, https://doi.org/10.1002/adma.202209654.

[32] Jin, J.; Han, X.; Fang, Y. Y.; Zhang, Z. D.; Li, Y. P.; Zhang, T. Y.; Han, A. J.; Liu, J. F. Microenvironment engineering of Ru single-atom catalysts by regulating the cation vacancies in NiFe-layered double hydroxides. *Adv. Funct. Mater.* **2022**, *32*, 2109218.

[33] Qin, R. X.; Liu, K. L.; Wu, Q. Y.; Zheng, N. F. Surface coordination chemistry of atomically dispersed metal catalysts. *Chem. Rev.* **2020**, *120*, 11810–11899.

[34] Deng, D. H.; Chen, X. Q.; Yu, L.; Wu, X.; Liu, Q. F.; Liu, Y.; Yang, H. X.; Tian, H. F.; Hu, Y. F.; Du, P. P. et al. A single iron site confined in a graphene matrix for the catalytic oxidation of benzene at room temperature. *Sci. Adv.* **2015**, *1*, e1500462.

[35] Zhuang, Z. C.; Li, Y. H.; Yu, R. H.; Xia, L. X.; Yang, J. R.; Lang, Z. Q.; Zhu, J. X.; Huang, J. Z.; Wang, J. O.; Wang, Y. et al. Reversely trapping atoms from a perovskite surface for high-performance and durable fuel cell cathodes. *Nat. Catal.* **2022**, *5*, 300–310.

[36] Han, X.; Zhang, T. Y.; Wang, X. H.; Zhang, Z. D.; Li, Y. P.; Qin, Y. J.; Wang, B. Q.; Han, A. J.; Liu, J. F. Hollow mesoporous atomically dispersed metal-nitrogen-carbon catalysts with enhanced diffusion for catalysis involving larger molecules. *Nat. Commun.* **2022**, *13*, 2900.

[37] Li, R. Z.; Wang, D. S. Superiority of dual-atom catalysts in electrocatalysis: One step further than single-atom catalysts. *Adv. Energy Mater.* **2022**, *12*, 2103564.

[38] Cui, T. T.; Wang, Y. P.; Ye, T.; Wu, J.; Chen, Z. Q.; Li, J.; Lei, Y. P.; Wang, D. S.; Li, Y. D. Engineering dual single-atom sites on 2D ultrathin N-doped carbon nanosheets attaining ultra-low-temperature zinc-air battery. *Angew. Chem., Int. Ed.* **2022**, *61*, e202115219.

[39] Sun, Z. G.; Zhang, H. J.; Cao, L. L.; Liu, X. K.; Wu, D.; Shen, X. Y.; Zhang, X.; Chen, Z. H.; Ru, S.; Zhu, X. Y. et al. Understanding synergistic catalysis on Cu-Se dual atom sites via *operando* X-ray absorption spectroscopy in oxygen reduction reaction. *Angew. Chem., Int. Ed.* **2023**, *62*, e202217719.

[40] Liang, X. M.; Wang, H. J.; Zhang, C.; Zhong, D. C.; Lu, T. B. Controlled synthesis of a Ni₂ dual-atom catalyst for synergistic CO_2 electroreduction. *Appl. Catal. B: Environ.* **2023**, *322*, 122073.

[41] Wang, Y.; Wu, J.; Tang, S. H.; Yang, J. R.; Ye, C. L.; Chen, J.; Lei, Y. P.; Wang, D. S. Synergistic Fe–Se atom pairs as bifunctional oxygen electrocatalysts boost low-temperature rechargeable Zn-air battery. *Angew. Chem., Int. Ed.* **2023**, *62*, e202219191.

[42] Dong, C. Y.; Gao, Z. R.; Li, Y. L.; Peng, M.; Wang, M.; Xu, Y.; Li, C. Y.; Xu, M.; Deng, Y. C.; Qin, X. T. et al. Fully exposed palladium cluster catalysts enable hydrogen production from nitrogen heterocycles. *Nat. Catal.* **2022**, *5*, 485–493.

[43] Zhang, L. L.; Liu, L.; Pan, Z. Y.; Zhang, R.; Gao, Z. Y.; Wang, G. M.; Huang, K. K.; Mu, X. Y.; Bai, F. Q.; Wang, Y. et al. Visible-light-driven non-oxidative dehydrogenation of alkanes at ambient conditions. *Nat. Energy* **2022**, *7*, 1042–1051.

[44] Jeong, H.; Kwon, O.; Kim, B. S.; Bae, J.; Shin, S.; Kim, H. E.; Kim, J.; Lee, H. Highly durable metal ensemble catalysts with full dispersion for automotive applications beyond single-atom catalysts. *Nat. Catal.* **2020**, *3*, 368–375.

[45] Jeong, H.; Lee, G.; Kim, B. S.; Bae, J.; Han, J. W.; Lee, H. Fully dispersed Rh ensemble catalyst to enhance low-temperature activity. *J. Am. Chem. Soc.* **2018**, *140*, 9558–9565.

[46] Zhang, J.; Wang, M.; Gao, Z. R.; Qin, X. T.; Xu, Y.; Wang, Z. H.; Zhou, W.; Ma, D. Importance of species heterogeneity in supported metal catalysts. *J. Am. Chem. Soc.* **2022**, *144*, 5108–5115.

[47] An, Z.; Zhang, Z. L.; Huang, Z. Y.; Han, H. B.; Song, B. B.; Zhang, J.; Ping, Q.; Zhu, Y. R.; Song, H. Y.; Wang, B. et al. Pt₁ enhanced C-H activation synergistic with Pt$_n$ catalysis for glycerol cascade oxidation to glyceric acid. *Nat. Commun.* **2022**, *13*, 5467.

[48] Liang, X.; Fu, N. H.; Yao, S. C.; Li, Z.; Li, Y. D. The progress and

outlook of metal single-atom-site catalysis. *J. Am. Chem. Soc.* **2022**, *144*, 18155–18174.

[49] Zheng, X. B.; Li, B. B.; Wang, Q. S.; Wang, D. S.; Li, Y. D. Emerging low-nuclearity supported metal catalysts with atomic level precision for efficient heterogeneous catalysis. *Nano Res.* **2022**, *15*, 7806–7839.

[50] He, C.; Cheng, J.; Zhang, X.; Douthwaite, M.; Pattisson, S.; Hao, Z. P. Recent advances in the catalytic oxidation of volatile organic compounds: A review based on pollutant sorts and sources. *Chem. Rev.* **2019**, *119*, 4471–4568.

[51] Chen, G. X.; Zhao, Y.; Fu, G.; Duchesne, P. N.; Gu, L.; Zheng, Y. P.; Weng, X. F.; Chen, M. S.; Zhang, P.; Pao, C. W. et al. Interfacial effects in iron-nickel hydroxide-platinum nanoparticles enhance catalytic oxidation. *Science* **2014**, *344*, 495–499.

[52] Yan, X. L.; Gan, T.; Shi, S. Z.; Du, J.; Xu, G. H.; Zhang, W. X.; Yan, W. F.; Zou, Y. C.; Liu, G. Potassium-incorporated manganese oxide enhances the activity and durability of platinum catalysts for low-temperature CO oxidation. *Catal. Sci. Technol.* **2021**, *11*, 6369–6373.

[53] Zheng, B.; Gan, T.; Shi, S. Z.; Wang, J. H.; Zhang, W. X.; Zhou, X.; Zou, Y. C.; Yan, W. F.; Liu, G. Exsolution of iron oxide on LaFeO3 perovskite: A robust heterostructured support for constructing self-adjustable Pt-based room-temperature CO oxidation catalysts. *ACS Appl. Mater. Interfaces* **2021**, *13*, 27029–27040.

[54] Muravev, V.; Spezzati, G.; Su, Y. Q.; Parastaev, A.; Chiang, F. K.; Longo, A.; Escudero, C.; Kosinov, N.; Hensen, E. J. M. Interface dynamics of Pd-CeO2 single-atom catalysts during CO oxidation. *Nat. Catal.* **2021**, *4*, 469–478.

[55] Wu, C. H.; Liu, C.; Su, D.; Xin, H. L.; Fang, H. T.; Eren, B.; Zhang, S.; Murray, C. B.; Salmeron, M. B. Bimetallic synergy in cobalt-palladium nanocatalysts for CO oxidation. *Nat. Catal.* **2018**, *2*, 78–85.

[56] Xu, H. D.; Zhang, Z. H.; Liu, J. X.; Do-Thanh, C. L.; Chen, H.; Xu, S. H.; Lin, Q. J.; Jiao, Y.; Wang, J. L.; Wang, Y. et al. Entropy-stabilized single-atom Pd catalysts via high-entropy fluorite oxide supports. *Nat. Commun.* **2020**, *11*, 3908.

[57] Maurer, F.; Jelic, J.; Wang, J. J.; Gänzler, A.; Dolcet, P.; Wöll, C.; Wang, Y. M.; Studt, F.; Casapu, M.; Grunwaldt, J. D. Tracking the formation, fate and consequence for catalytic activity of Pt single sites on CeO2. *Nat. Catal.* **2020**, *3*, 824–833.

[58] Pereira-Hernández, X. I.; DeLaRiva, A.; Muravev, V.; Kunwar, D.; Xiong, H. F.; Suddith, B.; Engelhard, M.; Kovarik, L.; Hensen, E. J. M.; Wang, Y. et al. Tuning Pt–CeO2 interactions by high-temperature vapor-phase synthesis for improved reducibility of lattice oxygen. *Nat. Commun.* **2019**, *10*, 1358.

[59] Kothari, M.; Jeon, Y.; Miller, D. N.; Pascui, A. E.; Kilmartin, J.; Wails, D.; Ramos, S.; Chadwick, A.; Irvine, J. T. S. Platinum incorporation into titanate perovskites to deliver emergent active and stable platinum nanoparticles. *Nat. Chem.* **2021**, *13*, 677–682.

[60] Wang, Y.; Ren, P. J.; Hu, J. T.; Tu, Y. C.; Gong, Z. M.; Cui, Y.; Zheng, Y. P.; Chen, M. S.; Zhang, W. J.; Ma, C. et al. Electron penetration triggering interface activity of Pt-graphene for CO oxidation at room temperature. *Nat. Commun.* **2021**, *12*, 5814.

[61] Haruta, M.; Yamada, N.; Kobayashi, T.; Iijima, S. Gold catalysts prepared by coprecipitation for low-temperature oxidation of hydrogen and of carbon monoxide. *J. Catal.* **1989**, *115*, 301–309.

[62] Wan, J. W.; Chen, W. X.; Jia, C. Y.; Zheng, L. R.; Dong, J. C.; Zheng, X. S.; Wang, Y.; Yan, W. S.; Chen, C.; Peng, Q. et al. Defect effects on TiO2 nanosheets: Stabilizing single atomic site Au and promoting catalytic properties. *Adv. Mater.* **2018**, *30*, 1705369.

[63] Fang, Y. R.; Zhang, Q.; Zhang, H.; Li, X. M.; Chen, W.; Xu, J.; Shen, H.; Yang, J.; Pan, C. Q.; Zhu, Y. H. et al. Dual activation of molecular oxygen and surface lattice oxygen in single atom Cu1/TiO2 catalyst for CO oxidation. *Angew. Chem., Int. Ed.* **2022**, *61*, e202212273.

[64] Yu, W. Z.; Wang, W. W.; Li, S. Q.; Fu, X. P.; Wang, X.; Wu, K.; Si, R.; Ma, C.; Jia, C. J.; Yan, C. H. Construction of active site in a sintered copper-ceria nanorod catalyst. *J. Am. Chem. Soc.* **2019**, *141*, 17548–17557.

[65] Kwak, J. H.; Hu, J. Z.; Mei, D. H.; Yi, C. W.; Kim, D. H.; Peden, C. H. F.; Allard, L. F.; Szanyi, J. Coordinatively unsaturated Al3+ centers as binding sites for active catalyst phases of platinum on γ-Al2O3. *Science* **2009**, *325*, 1670–1673.

[66] Jones, J.; Xiong, H. F.; DeLaRiva, A. T.; Peterson, E. J.; Pham, H.; Challa, S. R.; Qi, G.; Oh, S.; Wiebenga, M. H.; Hernández, X. I. P. et al. Thermally stable single-atom platinum-on-ceria catalysts via atom trapping. *Science* **2016**, *353*, 150–154.

[67] Nie, L.; Mei, D. H.; Xiong, H. F.; Peng, B.; Ren, Z. B.; Hernandez, X. I. P.; DeLaRiva, A.; Wang, M.; Engelhard, M. H.; Kovarik, L. et al. Activation of surface lattice oxygen in single-atom Pt/CeO2 for low-temperature CO oxidation. *Science* **2017**, *358*, 1419–1423.

[68] Li, X.; Pereira-Hernández, X. I.; Chen, Y. Z.; Xu, J.; Zhao, J. K.; Pao, C. W.; Fang, C. Y.; Zeng, J.; Wang, Y.; Gates, B. C. et al. Functional CeOx nanoglues for robust atomically dispersed catalysts. *Nature* **2022**, *611*, 284–288.

[69] Cao, L. N.; Liu, W.; Luo, Q. Q.; Yin, R. T.; Wang, B.; Weissenrieder, J.; Soldemo, M.; Yan, H.; Lin, Y.; Sun, Z. H. et al. Atomically dispersed iron hydroxide anchored on Pt for preferential oxidation of CO in H2. *Nature* **2019**, *565*, 631–635.

[70] DeRita, L.; Resasco, J.; Dai, S.; Boubnov, A.; Thang, H. V.; Hoffman, A. S.; Ro, I.; Graham, G. W.; Bare, S. R.; Pacchioni, G. et al. Structural evolution of atomically dispersed Pt catalysts dictates reactivity. *Nat. Mater.* **2019**, *18*, 746–751.

[71] Kunwar, D.; Zhou, S. L.; DeLaRiva, A.; Peterson, E. J.; Xiong, H. F.; Pereira-Hernández, X. I.; Purdy, S. C.; Ter Veen, R.; Brongersma, H. H.; Miller, J. T. et al. Stabilizing high metal loadings of thermally stable platinum single atoms on an industrial catalyst support. *ACS Catal.* **2019**, *9*, 3978–3990.

[72] Jiang, D.; Yao, Y. G.; Li, T. Y.; Wan, G.; Pereira-Hernández, X. I.; Lu, Y. B.; Tian, J. S.; Khivantsev, K.; Engelhard, M. H.; Sun, C. J. et al. Tailoring the local environment of platinum in single-atom Pt1/CeO2 catalysts for robust low-temperature CO oxidation. *Angew. Chem., Int. Ed.* **2021**, *60*, 26054–26062.

[73] Zhang, N. Q.; Ye, C. L.; Yan, H.; Li, L. C.; He, H.; Wang, D. S.; Li, Y. D. Single-atom site catalysts for environmental catalysis. *Nano Res.* **2020**, *13*, 3165–3182.

[74] Wang, F.; Ma, J.; Xin, S.; Wang, Q.; Xu, J.; Zhang, C.; He, H.; Zeng, X. C. Resolving the puzzle of single-atom silver dispersion on nanosized γ-Al2O3 surface for high catalytic performance. *Nat. Commun.* **2020**, *11*, 529.

[75] Lin, J.; Qiao, B. T.; Li, N.; Li, L.; Sun, X. C.; Liu, J. Y.; Wang, X. D.; Zhang, T. Little do more: A highly effective Pt1/FeOx single-atom catalyst for the reduction of NO by H2. *Chem. Commun.* **2015**, *51*, 7911–7914.

[76] Khivantsev, K.; Vargas, C. G.; Tian, J.; Kovarik, L.; Jaegers, N. R.; Szanyi, J.; Wang, Y. Economizing on precious metals in three-way catalysts: Thermally stable and highly active single-atom rhodium on ceria for NO abatement under dry and industrially relevant conditions. *Angew. Chem., Int. Ed.* **2021**, *60*, 391–398.

[77] Zhang, S. R.; Tang, Y.; Nguyen, L.; Zhao, Y. F.; Wu, Z. L.; Goh, T. W.; Liu, J. J.; Li, Y. Y.; Zhu, T.; Huang, W. Y. et al. Catalysis on singly dispersed Rh atoms anchored on an inert support. *ACS Catal.* **2018**, *8*, 110–121.

[78] Qu, W. Y.; Liu, X. N.; Chen, J. X.; Dong, Y. Y.; Tang, X. F.; Chen, Y. X. Single-atom catalysts reveal the dinuclear characteristic of active sites in NO selective reduction with NH3. *Nat. Commun.* **2020**, *11*, 1532.

[79] Beniya, A.; Higashi, S. Towards dense single-atom catalysts for future automotive applications. *Nat. Catal.* **2019**, *2*, 590–602.

[80] Farrauto, R. J.; Deeba, M.; Alerasool, S. Gasoline automobile catalysis and its historical journey to cleaner air. *Nat. Catal.* **2019**, *2*, 603–613.

[81] Datye, A. K.; Votsmeier, M. Opportunities and challenges in the development of advanced materials for emission control catalysts. *Nat. Mater.* **2021**, *20*, 1049–1059.

[82] Zhou, X.; Han, K.; Li, K.; Pan, J.; Wang, X.; Shi, W. D.; Song, S. Y.; Zhang, H. J. Dual-site single-atom catalysts with high performance for three-way catalysis. *Adv. Mater.* **2022**, *34*, 2201859.

[83] Kamal, M. S.; Razzak, S. A.; Hossain, M. M. Catalytic oxidation of

volatile organic compounds (VOCs)—A review. *Atmos. Environ.* **2016**, *140*, 117–134.

[84] Yang, W. H.; Peng, Y.; Wang, Y.; Wang, Y.; Liu, H.; Su, Z. A.; Yang, W. N.; Chen, J. J.; Si, W. Z.; Li, J. H. Controllable redox-induced *in-situ* growth of MnO₂ over Mn₂O₃ for toluene oxidation: Active heterostructure interfaces. *Appl. Catal. B: Environ.* **2020**, *278*, 119279.

[85] Yang, Q. L.; Wang, X. Y.; Wang, H. L.; Li, X. B.; Li, Q.; Wu, Y. M.; Peng, Y.; Ma, Y. L.; Li, J. H. Surface tailoring on SrMnO₃@SmMn₂O₅ for boosting the performance in diesel oxidation catalyst. *Appl. Catal. B: Environ.* **2023**, *320*, 121993.

[86] Chen, J.; Yan, D. X.; Xu, Z.; Chen, X.; Chen, X.; Xu, W. J.; Jia, H. P.; Chen, J. A novel redox precipitation to synthesize Au-doped α-MnO₂ with high dispersion toward low-temperature oxidation of formaldehyde. *Environ. Sci. Technol.* **2018**, *52*, 4728–4737.

[87] Hu, P. P.; Huang, Z. W.; Amghouz, Z.; Makkee, M.; Xu, F.; Kapteijn, F.; Dikhtiarenko, A.; Chen, Y. X.; Gu, X.; Tang, X. F. Electronic metal–support interactions in single-atom catalysts. *Angew. Chem., Int. Ed.* **2014**, *53*, 3418–3421.

[88] Gan, T.; Yang, J. X.; Morris, D.; Chu, X. F.; Zhang, P.; Zhang, W. X.; Zou, Y. C.; Yan, W. F.; Wei, S. H.; Liu, G. Electron donation of non-oxide supports boosts O₂ activation on nano-platinum catalysts. *Nat. Commun.* **2021**, *12*, 2741.

[89] Yang, K.; Liu, Y. X.; Deng, J. G.; Zhao, X. T.; Yang, J.; Han, Z.; Hou, Z. Q.; Dai, H. X. Three-dimensionally ordered mesoporous iron oxide-supported single-atom platinum: Highly active catalysts for benzene combustion. *Appl. Catal. B: Environ.* **2019**, *244*, 650–659.

[90] Yan, D. X.; Chen, J.; Jia, H. P. Temperature-induced structure reconstruction to prepare a thermally stable single-atom platinum catalyst. *Angew. Chem., Int. Ed.* **2020**, *59*, 13562–13567.

[91] Zhang, H. Y.; Sui, S. H.; Zheng, X. M.; Cao, R. R.; Zhang, P. Y. One-pot synthesis of atomically dispersed Pt on MnO₂ for efficient catalytic decomposition of toluene at low temperatures. *Appl. Catal. B: Environ.* **2019**, *257*, 117878.

[92] Hou, Z. Q.; Dai, L. Y.; Deng, J. G.; Zhao, G. F.; Jing, L.; Wang, Y. S.; Yu, X. H.; Gao, R. Y.; Tian, X. R.; Dai, H. X. et al. Electronically engineering water resistance in methane combustion with an atomically dispersed tungsten on PdO catalyst. *Angew. Chem., Int. Ed.* **2022**, *61*, e202201655.

[93] Zhuang, Z. W.; Wang, Y.; Xu, C. Q.; Liu, S. J.; Chen, C.; Peng, Q.; Zhuang, Z. B.; Xiao, H.; Pan, Y.; Lu, S. Q. et al. Three-dimensional open nano-netcage electrocatalysts for efficient pH-universal overall water splitting. *Nat. Commun.* **2019**, *10*, 4875.

[94] Jiang, Z. L.; Song, S. J.; Zheng, X. B.; Liang, X.; Li, Z. X.; Gu, H. F.; Li, Z.; Wang, Y.; Liu, S. H.; Chen, W. X. et al. Lattice strain and Schottky junction dual regulation boosts ultrafine ruthenium nanoparticles anchored on a N-modified carbon catalyst for H₂ production. *J. Am. Chem. Soc.* **2022**, *144*, 19619–19626.

[95] Cheng, J. L.; Wang, D. S. 2D materials modulating layered double hydroxides for electrocatalytic water splitting. *Chin. J. Catal.* **2022**, *43*, 1380–1398.

[96] Li, Y. P.; Wang, W. T.; Cheng, M. Y.; Feng, Y. F.; Han, X.; Qian, Q. Z.; Zhu, Y.; Zhang, G. Q. Arming Ru with oxygen vacancy enriched RuO₂ sub-nanometer skin activates superior bifunctionality for pH-universal overall water splitting. *Adv. Mater.*, in press, https://doi.org/10.1002/adma.202206351.

[97] Wang, Y.; Zheng, X. B.; Wang, D. S. Design concept for electrocatalysts. *Nano Res.* **2021**, *15*, 1730–1752.

[98] Jing, H. Y.; Zhu, P.; Zheng, X. B.; Zhang, Z. D.; Wang, D. S.; Li, Y. D. Theory-oriented screening and discovery of advanced energy transformation materials in electrocatalysis. *Adv. Powder Mater.* **2022**, *1*, 100013.

[99] Liu, Z. H.; Du, Y.; Yu, R. H.; Zheng, M. B.; Hu, R.; Wu, J. S.; Xia, Y. Y.; Zhuang, Z. C.; Wang, D. S. Tuning mass transport in electrocatalysis down to sub-5 nm through nanoscale grade separation. *Angew. Chem., Int. Ed.* **2023**, *62*, e202212653.

[100] Yang, Q.; Liu, H. X.; Yuan, P.; Jia, Y.; Zhuang, L. Z.; Zhang, H. W.; Yan, X. C.; Liu, G. H.; Zhao, Y. F.; Liu, J. Z. et al. Single carbon vacancy traps atomic platinum for hydrogen evolution catalysis. *J. Am. Chem. Soc.* **2022**, *144*, 2171–2178.

[101] Liu, F.; Shi, C. X.; Guo, X. L.; He, Z. X.; Pan, L.; Huang, Z. F.; Zhang, X. W.; Zou, J. J. Rational design of better hydrogen evolution electrocatalysts for water splitting: A review. *Adv. Sci. (Weinh.)* **2022**, *9*, 2200307.

[102] Zheng, Y.; Jiao, Y.; Vasileff, A.; Qiao, S. Z. The hydrogen evolution reaction in alkaline solution: From theory, single crystal models, to practical electrocatalysts. *Angew. Chem., Int. Ed.* **2018**, *57*, 7568–7579.

[103] Zhou, A. W.; Wang, D. S.; Li, Y. D. Hollow microstructural regulation of single-atom catalysts for optimized electrocatalytic performance. *Microstructures* **2022**, *2*, 2022005.

[104] Zhu, P.; Xiong, X.; Wang, D. S. Regulations of active moiety in single atom catalysts for electrochemical hydrogen evolution reaction. *Nano Res.* **2022**, *15*, 5792–5815.

[105] Yang, J. R.; Li, W. H.; Tan, S. D.; Xu, K. N.; Wang, Y.; Wang, D. S.; Li, Y. D. The electronic metal–support interaction directing the design of single atomic site catalysts: Achieving high efficiency towards hydrogen evolution. *Angew. Chem., Int. Ed.* **2021**, *60*, 19085–19091.

[106] Zhao, Y. F.; Kumar, P. V.; Tan, X.; Lu, X. X.; Zhu, X. F.; Jiang, J. J.; Pan, J.; Xi, S. B.; Yang, H. Y.; Ma, Z. P. et al. Modulating Pt-O-Pt atomic clusters with isolated cobalt atoms for enhanced hydrogen evolution catalysis. *Nat. Commun.* **2022**, *13*, 2430.

[107] Zhang, T. Y.; Jin, J.; Chen, J. M.; Fang, Y. Y.; Han, X.; Chen, J. Y.; Li, Y. P.; Wang, Y.; Liu, J. F.; Wang, L. Pinpointing the axial ligand effect on platinum single-atom-catalyst towards efficient alkaline hydrogen evolution reaction. *Nat. Commun.* **2022**, *13*, 6875.

[108] Yu, F. Y.; Lang, Z. L.; Yin, L. Y.; Feng, K.; Xia, Y. J.; Tan, H. Q.; Zhu, H. T.; Zhong, J.; Kang, Z. H.; Li, Y. G. Pt–O bond as an active site superior to Pt⁰ in hydrogen evolution reaction. *Nat. Commun.* **2020**, *11*, 490.

[109] Liu, D. B.; Li, X. Y.; Chen, S. M.; Yan, H.; Wang, C. D.; Wu, C. Q.; Haleem, Y. A.; Duan, S.; Lu, J. L.; Ge, B. H. et al. Atomically dispersed platinum supported on curved carbon supports for efficient electrocatalytic hydrogen evolution. *Nat. Energy* **2019**, *4*, 512–518.

[110] Shi, Y.; Ma, Z. R.; Xiao, Y. Y.; Yin, Y. C.; Huang, W. M.; Huang, Z. C.; Zheng, Y. Z.; Mu, F. Y.; Huang, R.; Shi, G. Y. et al. Electronic metal–support interaction modulates single-atom platinum catalysis for hydrogen evolution reaction. *Nat. Commun.* **2021**, *12*, 3021.

[111] Wang, Q. L.; Cheng, Y. Q.; Tao, H. B.; Liu, Y. H.; Ma, X. H.; Li, D. S.; Yang, H. B.; Liu, B. Long-term stability challenges and opportunities in acidic oxygen evolution electrocatalysis. *Angew. Chem., Int. Ed.* **2023**, *62*, e202216645.

[112] Zhu, H.; Sun, S. H.; Hao, J. C.; Zhuang, Z. C.; Zhang, S. G.; Wang, T. D.; Kang, Q.; Lu, S. L.; Wang, X. F.; Lai, F. L. et al. A high-entropy atomic environment converts inactive to active sites for electrocatalysis. *Energy Environ. Sci.* **2023**, *16*, 619–628.

[113] Liu, X. H.; Xi, S. B.; Kim, H.; Kumar, A.; Lee, J.; Wang, J.; Tran, N. Q.; Yang, T.; Shao, X. D.; Liang, M. F. et al. Restructuring highly electron-deficient metal-metal oxides for boosting stability in acidic oxygen evolution reaction. *Nat. Commun.* **2021**, *12*, 5676.

[114] Wu, D. S.; Kusada, K.; Yoshioka, S.; Yamamoto, T.; Toriyama, T.; Matsumura, S.; Chen, Y. N.; Seo, O.; Kim, J.; Song, C. et al. Efficient overall water splitting in acid with anisotropic metal nanosheets. *Nat. Commun.* **2021**, *12*, 1145.

[115] Zu, L. H.; Qian, X. Y.; Zhao, S. L.; Liang, Q. H.; Chen, Y. E.; Liu, M.; Su, B. J.; Wu, K. H.; Qu, L. B.; Duan, L. L. et al. Self-assembly of Ir-based nanosheets with ordered interlayer space for enhanced electrocatalytic water oxidation. *J. Am. Chem. Soc.* **2022**, *144*, 2208–2217.

[116] Li, S.; Chen, B. B.; Wang, Y.; Ye, M. Y.; Van Aken, P. A.; Cheng, C.; Thomas, A. Oxygen-evolving catalytic atoms on metal carbides. *Nat. Mater.* **2021**, *20*, 1240–1247.

[117] Cao, L. L.; Luo, Q. Q.; Chen, J. J.; Wang, L.; Lin, Y.; Wang, H. J.; Liu, X. K.; Shen, X. Y.; Zhang, W.; Liu, W. et al. Dynamic oxygen adsorption on single-atomic ruthenium catalyst with high

performance for acidic oxygen evolution reaction. *Nat. Commun.* **2019**, *10*, 4849.

[118] Zheng, X. B.; Yang, J. R.; Xu, Z. F.; Wang, Q. S.; Wu, J. B.; Zhang, E. H.; Dou, S. X.; Sun, W. P.; Wang, D. S.; Li, Y. D. Ru–Co pair sites catalyst boosts the energetics for the oxygen evolution reaction. *Angew. Chem., Int. Ed.* **2022**, *61*, e202205946.

[119] Yao, Y. C.; Hu, S. L.; Chen, W. X.; Huang, Z. Q.; Wei, W. C.; Yao, T.; Liu, R. R.; Zang, K. T.; Wang, X. Q.; Wu, G. et al. Engineering the electronic structure of single atom Ru sites via compressive strain boosts acidic water oxidation electrocatalysis. *Nat. Catal.* **2019**, *2*, 304–313.

[120] Jiang, K.; Luo, M.; Peng, M.; Yu, Y. Q.; Lu, Y. R.; Chan, T. S.; Liu, P.; De Groot, F. M. F.; Tan, Y. W. Dynamic active-site generation of atomic iridium stabilized on nanoporous metal phosphides for water oxidation. *Nat. Commun.* **2020**, *11*, 2701.

[121] Bai, L. C.; Hsu, C. S.; Alexander, D. T. L.; Chen, H. M.; Hu, X. L. Double-atom catalysts as a molecular platform for heterogeneous oxygen evolution electrocatalysis. *Nat. Energy* **2021**, *6*, 1054–1066.

[122] Zeng, Z. P.; Gan, L. Y.; Yang, H. B.; Su, X. Z.; Gao, J. J.; Liu, W.; Matsumoto, H.; Gong, J.; Zhang, J. M.; Cai, W. Z. et al. Orbital coupling of hetero-diatomic nickel-iron site for bifunctional electrocatalysis of CO_2 reduction and oxygen evolution. *Nat. Commun.* **2021**, *12*, 4088.

[123] Wang, Y.; Wang, D. S.; Li, Y. D. A fundamental comprehension and recent progress in advanced Pt-based ORR nanocatalysts. *SmartMat* **2021**, *2*, 56–75.

[124] Zhuang, Z. C.; Kang, Q.; Wang, D. S.; Li, Y. D. Single-atom catalysis enables long-life, high-energy lithium-sulfur batteries. *Nano Res.* **2020**, *13*, 1856–1866.

[125] Wang, Y.; Wang, D. S.; Li, Y. D. Rational design of single-atom site electrocatalysts: From theoretical understandings to practical applications. *Adv. Mater.* **2021**, *33*, 2008151.

[126] Chen, Y. J.; Gao, R.; Ji, S. F.; Li, H. J.; Tang, K.; Jiang, P.; Hu, H. B.; Zhang, Z. D.; Hao, H. G.; Qu, Q. Y. et al. Atomic-level modulation of electronic density at cobalt single-atom sites derived from metal-organic frameworks: Enhanced oxygen reduction performance. *Angew. Chem., Int. Ed.* **2021**, *60*, 3212–3221.

[127] Han, A. L.; Wang, X. J.; Tang, K.; Zhang, Z. D.; Ye, C. L.; Kong, K. J.; Hu, H. B.; Zheng, L. R.; Jiang, P.; Zhao, C. X. et al. An adjacent atomic platinum site enables single-atom iron with high oxygen reduction reaction performance. *Angew. Chem., Int. Ed.* **2021**, *60*, 19262–19271.

[128] Zhuang, Z. C.; Xia, L. X.; Huang, J. Z.; Zhu, P.; Li, Y.; Ye, C. L.; Xia, M. G.; Yu, R. H.; Lang, Z. Q.; Zhu, J. X. et al. Continuous modulation of electrocatalytic oxygen reduction activities of single-atom catalysts through p-n junction rectification. *Angew. Chem., Int. Ed.* **2023**, *62*, e202212335.

[129] Zhuang, Z. C.; Li, Y.; Li, Y. H.; Huang, J. Z.; Wei, B.; Sun, R.; Ren, Y. J.; Ding, J.; Zhu, J. X.; Lang, Z. Q. et al. Atomically dispersed nonmagnetic electron traps improve oxygen reduction activity of perovskite oxides. *Energy Environ. Sci.* **2021**, *14*, 1016–1028.

[130] Liu, J.; Jiao, M. G.; Mei, B. B.; Tong, Y. X.; Li, Y. P.; Ruan, M. B.; Song, P.; Sun, G. Q.; Jiang, L. H.; Wang, Y. et al. Carbon-supported divacancy-anchored platinum single-atom electrocatalysts with superhigh Pt utilization for the oxygen reduction reaction. *Angew. Chem., Int. Ed.* **2019**, *58*, 1163–1167.

[131] Song, Z. X.; Zhu, Y. N.; Liu, H. S.; Banis, M. N.; Zhang, L.; Li, J. J.; Doyle-Davis, K.; Li, R. Y.; Sham, T. K.; Yang, L. J. et al. Engineering the low coordinated Pt single atom to achieve the superior electrocatalytic performance toward oxygen reduction. *Small* **2020**, *16*, 2003096.

[132] Gao, R. J.; Wang, J.; Huang, Z. F.; Zhang, R. R.; Wang, W.; Pan, L.; Zhang, J. F.; Zhu, W. K.; Zhang, X. W.; Shi, C. X. et al. Pt/Fe_2O_3 with Pt–Fe pair sites as a catalyst for oxygen reduction with ultralow Pt loading. *Nat. Energy* **2021**, *6*, 614–623.

[133] Han, X.; Zhang, T. Y.; Chen, W. X.; Dong, B.; Meng, G.; Zheng, L. R.; Yang, C.; Sun, X. M.; Zhuang, Z. B.; Wang, D. S. et al. Mn-N_4 oxygen reduction electrocatalyst: *Operando* investigation of active sites and high performance in zinc-air battery. *Adv. Energy Mater.* **2021**, *11*, 2002753.

[134] Jin, Z. Y.; Li, P. P.; Meng, Y.; Fang, Z. W.; Xiao, D.; Yu, G. H. Understanding the inter-site distance effect in single-atom catalysts for oxygen electroreduction. *Nat. Catal.* **2021**, *4*, 615–622.

[135] Chang, Q. W.; Zhang, P.; Mostaghimi, A. H. B.; Zhao, X. R.; Denny, S. R.; Lee, J. H.; Gao, H. P.; Zhang, Y.; Xin, H. L.; Siahrostami, S. et al. Promoting H_2O_2 production via 2-electron oxygen reduction by coordinating partially oxidized Pd with defect carbon. *Nat. Commun.* **2020**, *11*, 2178.

[136] Yuan, Q. X.; Fan, M. M.; Zhao, Y. Y.; Wu, J. J.; Raj, J.; Wang, Z. M.; Wang, A.; Sun, H.; Xu, X.; Wu, Y. H. et al. Facile fabrication of carbon dots containing abundant h-BN/graphite heterostructures as efficient electrocatalyst for hydrogen peroxide synthesis. *Appl. Catal. B: Environ.* **2023**, *324*, 122195.

[137] Zheng, Y. J.; Wang, P.; Huang, W. H.; Chen, C. L.; Jia, Y. Y.; Dai, S.; Li, T.; Zhao, Y.; Qiu, Y. C.; Waterhouse, G. I. N. et al. Toward more efficient carbon-based electrocatalysts for hydrogen peroxide synthesis: Roles of cobalt and carbon defects in two-electron ORR catalysis. *Nano Lett.* **2023**, *23*, 1100–1108.

[138] Zhang, E. H.; Tao, L.; An, J. K.; Zhang, J. W.; Meng, L. Z.; Zheng, X. B.; Wang, Y.; Li, N.; Du, S. X.; Zhang, J. T. et al. Engineering the local atomic environments of indium single-atom catalysts for efficient electrochemical production of hydrogen peroxide. *Angew. Chem., Int. Ed.* **2022**, *61*, e202117347.

[139] Jiang, K.; Back, S.; Akey, A. J.; Xia, C.; Hu, Y. F.; Liang, W. T.; Schaak, D.; Stavitski, E.; Nørskov, J. K.; Siahrostami, S. et al. Highly selective oxygen reduction to hydrogen peroxide on transition metal single atom coordination. *Nat. Commun.* **2019**, *10*, 3997.

[140] Qiu, Y. J.; Zhang, J.; Jin, J.; Sun, J. Q.; Tang, H. L.; Chen, Q. Q.; Zhang, Z. D.; Sun, W. M.; Meng, G.; Xu, Q. et al. Construction of Pd-Zn dual sites to enhance the performance for ethanol electro-oxidation reaction. *Nat. Commun.* **2021**, *12*, 5273.

[141] Duchesne, P. N.; Li, Z. Y.; Deming, C. P.; Fung, V.; Zhao, X. J.; Yuan, J.; Regier, T.; Aldalbahi, A.; Almarhoon, Z.; Chen, S. W. et al. Golden single-atomic-site platinum electrocatalysts. *Nat. Mater.* **2018**, *17*, 1033–1039.

[142] Kim, J.; Roh, C. W.; Sahoo, S. K.; Yang, S.; Bae, J.; Han, J. W.; Lee, H. Highly durable platinum single-atom alloy catalyst for electrochemical reactions. *Adv. Energy Mater.* **2018**, *8*, 1701476.

[143] Qi, Y. B.; Zhang, Y.; Yang, L.; Zhao, Y. H.; Zhu, Y. H.; Jiang, H. L.; Li, C. Z. Insights into the activity of nickel boride/nickel heterostructures for efficient methanol electrooxidation. *Nat. Commun.* **2022**, *13*, 4602.

[144] Wang, Y.; Zheng, M.; Li, Y. R.; Ye, C. L.; Chen, J.; Ye, J. Y.; Zhang, Q. H.; Li, J.; Zhou, Z. Y.; Fu, X. Z. et al. p-d orbital hybridization induced by a monodispersed Ga site on a Pt_3Mn nanocatalyst boosts ethanol electrooxidation. *Angew. Chem., Int. Ed.* **2022**, *61*, e202115735.

[145] Li, M. F.; Duanmu, K. N.; Wan, C. Z.; Cheng, T.; Zhang, L.; Dai, S.; Chen, W. X.; Zhao, Z. P.; Li, P.; Fei, H. L. et al. Single-atom tailoring of platinum nanocatalysts for high-performance multifunctional electrocatalysis. *Nat. Catal.* **2019**, *2*, 495–503.

[146] Zhang, Z. Q.; Liu, J. P.; Wang, J.; Wang, Q.; Wang, Y. H.; Wang, K.; Wang, Z.; Gu, M.; Tang, Z. H.; Lim, J. et al. Single-atom catalyst for high-performance methanol oxidation. *Nat. Commun.* **2021**, *12*, 5235.

[147] Poerwoprajitno, A. R.; Gloag, L.; Watt, J.; Cheong, S.; Tan, X.; Lei, H.; Tahini, H. A.; Henson, A.; Subhash, B.; Bedford, N. M. et al. A single-Pt-atom-on-Ru-nanoparticle electrocatalyst for CO-resilient methanol oxidation. *Nat. Catal.* **2022**, *5*, 231–237.

[148] Xiong, Y.; Dong, J. C.; Huang, Z. Q.; Xin, P. Y.; Chen, W. X.; Wang, Y.; Li, Z.; Jin, Z.; Xing, W.; Zhuang, Z. B. et al. Single-atom Rh/N-doped carbon electrocatalyst for formic acid oxidation. *Nat. Nanotechnol.* **2020**, *15*, 390–397.

[149] Xu, A. N.; Hung, S. F.; Cao, A.; Wang, Z. B.; Karmodak, N.; Huang, J. E.; Yan, Y.; Rasouli, A. S.; Ozden, A.; Wu, F. Y. et al. Copper/alkaline earth metal oxide interfaces for electrochemical CO_2-to-alcohol conversion by selective hydrogenation. *Nat. Catal.* **2022**, *5*, 1081–1088.

[150] Ren, H. J.; Kovalev, M.; Weng, Z. Y.; Muhamad, M. Z.; Ma, H. Y.; Sheng, Y.; Sun, L. B.; Wang, J. J.; Rihm, S.; Yang, W. F. et al.

Operando proton-transfer-reaction time-of-flight mass spectrometry of carbon dioxide reduction electrocatalysis. *Nat. Catal.* **2022**, *5*, 1169–1179.

[151] Shin, S. J.; Choi, H.; Ringe, S.; Won, D. H.; Oh, H. S.; Kim, D. H.; Lee, T.; Nam, D. H.; Kim, H.; Choi, C. H. A unifying mechanism for cation effect modulating C1 and C2 productions from CO_2 electroreduction. *Nat. Commun.* **2022**, *13*, 5482.

[152] Zhu, J. W.; Wang, Y. Y.; Zhi, A. M.; Chen, Z. T.; Shi, L.; Zhang, Z. B.; Zhang, Y.; Zhu, Y. L.; Qiu, X. Y.; Tian, X. Z. et al. Cation-deficiency-dependent CO_2 electroreduction over copper-based ruddlesden-popper perovskite oxides. *Angew. Chem., Int. Ed.* **2022**, *61*, e202111670.

[153] Lin, L.; He, X. Y.; Zhang, X. G.; Ma, W. C.; Zhang, B.; Wei, D. Y.; Xie, S. J.; Zhang, Q. H.; Yi, X. D.; Wang, Y. A nanocomposite of bismuth clusters and $Bi_2O_2CO_3$ sheets for highly efficient electrocatalytic reduction of CO_2 to formate. *Angew. Chem., Int. Ed.* **2023**, *62*, e202214959.

[154] Xie, Y.; Ou, P. F.; Wang, X.; Xu, Z. Y.; Li, Y. C.; Wang, Z. Y.; Huang, J. E.; Wicks, J.; McCallum, C.; Wang, N. et al. High carbon utilization in CO_2 reduction to multi-carbon products in acidic media. *Nat. Catal.* **2022**, *5*, 564–570.

[155] Zhang, M. L.; Zhang, Z. D.; Zhao, Z. H.; Huang, H.; Anjum, D. H.; Wang, D. S.; He, J. H.; Huang, K. W. Tunable selectivity for electrochemical CO_2 reduction by bimetallic Cu-Sn catalysts: Elucidating the roles of Cu and Sn. *ACS Catal.* **2021**, *11*, 11103–11108.

[156] Zhang, Z. D.; Wang, D. S. Single-atom catalysts: Stimulating electrochemical CO_2 reduction reaction in the industrial era. *J. Mater. Chem. A* **2022**, *10*, 5863–5877.

[157] Zhang, N. Q.; Zhang, X. X.; Tao, L.; Jiang, P.; Ye, C. L.; Lin, R.; Huang, Z. W.; Li, A.; Pang, D. W.; Yan, H. et al. Silver single-atom catalyst for efficient electrochemical CO_2 reduction synthesized from thermal transformation and surface reconstruction. *Angew. Chem., Int. Ed.* **2021**, *60*, 6170–6176.

[158] Sun, X. H.; Tuo, Y.; Ye, C. L.; Chen, C.; Lu, Q.; Li, G. N.; Jiang, P.; Chen, S. H.; Zhu, P.; Ma, M. et al. Phosphorus induced electron localization of single iron sites for boosted CO_2 electroreduction reaction. *Angew. Chem., Int. Ed.* **2021**, *60*, 23614–23618.

[159] Zhang, N. Q.; Zhang, X. X.; Kang, Y. K.; Ye, C. L.; Jin, R.; Yan, H.; Lin, R.; Yang, J. R.; Xu, Q.; Wang, Y. et al. A supported Pd_2 dual-atom site catalyst for efficient electrochemical CO_2 reduction. *Angew. Chem., Int. Ed.* **2021**, *60*, 13388–13393.

[160] Zhang, Z. D.; Chen, S. H.; Zhu, J. X.; Ye, C. L.; Mao, Y.; Wang, B. Q.; Zhou, G.; Mai, L. Q.; Wang, Z. Y.; Liu, X. W. et al. Charge-separated $Pd^{\delta-}$–$Cu^{\delta+}$ atom pairs promote CO_2 reduction to C_2. *Nano Lett.* **2023**, *23*, 2312–2320.

[161] Chen, S. H.; Li, W. H.; Jiang, W. J.; Yang, J. R.; Zhu, J. X.; Wang, L. Q.; Ou, H. H.; Zhuang, Z. C.; Chen, M. Z.; Sun, X. H. et al. MOF encapsulating N-heterocyclic carbene-ligated copper single-atom site catalyst towards efficient methane electrosynthesis. *Angew. Chem., Int. Ed.* **2022**, *61*, e202114450.

[162] Zhang, Z. D.; Zhu, J. X.; Chen, S. H.; Sun, W. M.; Wang, D. S. Liquid fluxional Ga single atom catalysts for efficient electrochemical CO_2 reduction. *Angew. Chem., Int. Ed.* **2023**, *62*, e202215136.

[163] Wang, X. Q.; Chen, Z.; Zhao, X. Y.; Yao, T.; Chen, W. X.; You, R.; Zhao, C. M.; Wu, G.; Wang, J.; Huang, W. X. et al. Regulation of coordination number over single Co sites: Triggering the efficient electroreduction of CO_2. *Angew. Chem., Int. Ed.* **2018**, *57*, 1944–1948.

[164] Lin, Y. X.; Zhang, S. N.; Xue, Z. H.; Zhang, J. J.; Su, H.; Zhao, T. J.; Zhai, G. Y.; Li, X. H.; Antonietti, M.; Chen, J. S. Boosting selective nitrogen reduction to ammonia on electron-deficient copper nanoparticles. *Nat. Commun.* **2019**, *10*, 4380.

[165] Chen, G. F.; Yuan, Y. F.; Jiang, H. F.; Ren, S. Y.; Ding, L. X.; Ma, L.; Wu, T. P.; Lu, J.; Wang, H. H. Electrochemical reduction of nitrate to ammonia via direct eight-electron transfer using a copper-molecular solid catalyst. *Nat. Energy* **2020**, *5*, 605–613.

[166] Li, X. C.; Shen, P.; Luo, Y. J.; Li, Y. H.; Guo, Y. L.; Zhang, H.; Chu, K. PdFe single-atom alloy metallene for N_2 electroreduction. *Angew. Chem., Int. Ed.* **2022**, *61*, e202205923.

[167] Foster, S. L.; Bakovic, S. I. P.; Duda, R. D.; Maheshwari, S.; Milton, R. D.; Minteer, S. D.; Janik, M. J.; Renner, J. N.; Greenlee, L. F. Catalysts for nitrogen reduction to ammonia. *Nat. Catal.* **2018**, *1*, 490–500.

[168] Montoya, J. H.; Tsai, C.; Vojvodic, A.; Nørskov, J. K. The challenge of electrochemical ammonia synthesis: A new perspective on the role of nitrogen scaling relations. *ChemSusChem* **2015**, *8*, 2180–2186.

[169] Chen, C.; Zhu, X. R.; Wen, X. J.; Zhou, Y. Y.; Zhou, L.; Li, H.; Tao, L.; Li, Q. L.; Du, S. Q.; Liu, T. T. et al. Coupling N_2 and CO_2 in H_2O to synthesize urea under ambient conditions. *Nat. Chem.* **2020**, *12*, 717–724.

[170] Gu, Y.; Xi, B. J.; Tian, W. Z.; Zhang, H.; Fu, Q.; Xiong, S. L. Boosting selective nitrogen reduction via geometric coordination engineering on single-tungsten-atom catalysts. *Adv. Mater.* **2021**, *33*, 2100429.

[171] Li, Y.; Li, J. W.; Huang, J. H.; Chen, J. X.; Kong, Y.; Yang, B.; Li, Z. J.; Lei, L. C.; Chai, G. L.; Wen, Z. H. et al. Boosting electroreduction kinetics of nitrogen to ammonia via tuning electron distribution of single-atomic iron sites. *Angew. Chem., Int. Ed.* **2021**, *60*, 9078–9085.

[172] Zhang, S. B.; Han, M. M.; Shi, T. F.; Zhang, H. M.; Lin, Y.; Zheng, X. S.; Zheng, L. R.; Zhou, H. J.; Chen, C.; Zhang, Y. X. et al. Atomically dispersed bimetallic Fe-Co electrocatalysts for green production of ammonia. *Nat. Sustain.* **2023**, *6*, 169–179.

[173] Yan, H.; Su, C. L.; He, J.; Chen, W. Single-atom catalysts and their applications in organic chemistry. *J. Mater. Chem. A* **2018**, *6*, 8793–8814.

[174] Li, W. H.; Yang, J. R.; Wang, D. S.; Li, Y. D. Striding the threshold of an atom era of organic synthesis by single-atom catalysis. *Chem* **2022**, *8*, 119–140.

[175] Zhao, J.; Ji, S. F.; Guo, C. X.; Li, H. J.; Dong, J. C.; Guo, P.; Wang, D. S.; Li, Y. D.; Toste, F. D. A heterogeneous iridium single-atom-site catalyst for highly regioselective carbenoid O–H bond insertion. *Nat. Catal.* **2021**, *4*, 523–531.

[176] Chen, Z. P.; Vorobyeva, E.; Mitchell, S.; Fako, E.; Ortuño, M. A.; López, N.; Collins, S. M.; Midgley, P. A.; Richard, S.; Vilé, G. et al. A heterogeneous single-atom palladium catalyst surpassing homogeneous systems for Suzuki coupling. *Nat. Nanotechnol.* **2018**, *13*, 702–707.

[177] Li, W. H.; Ye, B. C.; Yang, J. R.; Wang, Y.; Yang, C. J.; Pan, Y. M.; Tang, H. T.; Wang, D. S.; Li, Y. D. A single-atom cobalt catalyst for the fluorination of acyl chlorides at parts-per-million catalyst loading. *Angew. Chem., Int. Ed.* **2022**, *61*, e202209749.

[178] Liu, P. X.; Zhao, Y.; Qin, R. X.; Mo, S. G.; Chen, G. X.; Gu, L.; Chevrier, D. M.; Zhang, P.; Guo, Q.; Zang, D. D. et al. Photochemical route for synthesizing atomically dispersed palladium catalysts. *Science* **2016**, *352*, 797–800.

[179] Wei, H. S.; Liu, X. Y.; Wang, A. Q.; Zhang, L. L.; Qiao, B. T.; Yang, X. F.; Huang, Y. Q.; Miao, S.; Liu, J. Y.; Zhang, T. FeO_x-supported platinum single-atom and pseudo-single-atom catalysts for chemoselective hydrogenation of functionalized nitroarenes. *Nat. Commun.* **2014**, *5*, 5634.

[180] Zhu, Y. Q.; Sun, W. M.; Luo, J.; Chen, W. X.; Cao, T.; Zheng, L. R.; Dong, J. C.; Zhang, J.; Zhang, M. L.; Han, Y. H. et al. A cocoon silk chemistry strategy to ultrathin N-doped carbon nanosheet with metal single-site catalysts. *Nat. Commun.* **2018**, *9*, 3861.

[181] Wang, L. B.; Zhang, W. B.; Wang, S. P.; Gao, Z. H.; Luo, Z. H.; Wang, X.; Zeng, R.; Li, A. W.; Li, H. L.; Wang, M. L. et al. Atomic-level insights in optimizing reaction paths for hydroformylation reaction over Rh/CoO single-atom catalyst. *Nat. Commun.* **2016**, *7*, 14036.

[182] Lang, R.; Li, T. B.; Matsumura, D.; Miao, S.; Ren, Y. J.; Cui, Y. T.; Tan, Y.; Qiao, B. T.; Li, L.; Wang, A. Q. et al. Hydroformylation of olefins by a rhodium single-atom catalyst with activity comparable to $RhCl(PPh_3)_3$. *Angew. Chem., Int. Ed.* **2016**, *55*, 16054–16058.

[183] Ro, I.; Qi, J.; Lee, S.; Xu, M. J.; Yan, X. X.; Xie, Z. H.; Zakem, G.; Morales, A.; Chen, J. G.; Pan, X. Q. et al. Bifunctional hydroformylation on heterogeneous Rh–WO_x pair site catalysts. *Nature* **2022**, *609*, 287–292.

[184] Yu, G. Y.; Qian, J.; Zhang, P.; Zhang, B.; Zhang, W. X.; Yan, W. F.; Liu, G. Collective excitation of plasmon-coupled Au-nanochain boosts photocatalytic hydrogen evolution of semiconductor. *Nat. Commun.* 2019, *10*, 4912.

[185] Schultz, D. M.; Yoon, T. P. Solar synthesis: Prospects in visible light photocatalysis. *Science* 2014, *343*, 1239176.

[186] Maeda, K.; Teramura, K.; Lu, D. L.; Takata, T.; Saito, N.; Inoue, Y.; Domen, K. Photocatalyst releasing hydrogen from water. *Nature* 2006, *440*, 295.

[187] Sivula, K.; Van De Krol, R. Semiconducting materials for photoelectrochemical energy conversion. *Nat. Rev. Mater.* 2016, *1*, 15010.

[188] Gao, C.; Low, J.; Long, R.; Kong, T. T.; Zhu, J. F.; Xiong, Y. J. Heterogeneous single-atom photocatalysts: Fundamentals and applications. *Chem. Rev.* 2020, *120*, 12175–12216.

[189] Li, X. G.; Bi, W. T.; Zhang, L.; Tao, S.; Chu, W. S.; Zhang, Q.; Luo, Y.; Wu, C. Z.; Xie, Y. Single-atom Pt as Co-catalyst for enhanced photocatalytic H_2 evolution. *Adv. Mater.* 2016, *28*, 2427–2431.

[190] Zhou, A. W.; Dou, Y. B.; Zhao, C.; Zhou, J.; Wu, X. Q.; Li, J. R. A leaf-branch TiO_2/carbon@MOF composite for selective CO_2 photoreduction. *Appl. Catal. B: Environ.* 2020, *264*, 118519.

[191] Wang, G.; Chen, Z.; Wang, T.; Wang, D. S.; Mao, J. J. P and Cu dual sites on graphitic carbon nitride for photocatalytic CO_2 reduction to hydrocarbon fuels with high C_2H_6 evolution. *Angew. Chem., Int. Ed.* 2022, *61*, e202210789.

[192] Wang, G.; Wu, Y.; Li, Z. J.; Lou, Z. Z.; Chen, Q. Q.; Li, Y. F.; Wang, D. S.; Mao, J. J. Engineering a copper single-atom electron bridge to achieve efficient photocatalytic CO_2 conversion. *Angew. Chem., Int. Ed.* 2023, *62*, e202218460.

[193] Ou, H. H.; Ning, S. B.; Zhu, P.; Chen, S. H.; Han, A. L.; Kang, Q.; Hu, Z. F.; Ye, J. H.; Wang, D. S.; Li, Y. D. Carbon nitride photocatalysts with integrated oxidation and reduction atomic active centers for improved CO_2 conversion. *Angew. Chem., Int. Ed.* 2022, *61*, e202206579.

[194] Liu, S. Z.; Wang, Y. J.; Wang, S. B.; You, M. M.; Hong, S.; Wu, T. S.; Soo, Y. L.; Zhao, Z. Q.; Jiang, G. Y.; Qiu, J. S. et al. Photocatalytic fixation of nitrogen to ammonia by single Ru atom decorated TiO_2 nanosheets. *ACS Sustainable Chem. Eng.* 2019, *7*, 6813–6820.

[195] Guo, X. W.; Chen, S. M.; Wang, H. J.; Zhang, Z. M.; Lin, H.; Song, L.; Lu, T. B. Single-atom molybdenum immobilized on photoactive carbon nitride as efficient photocatalysts for ambient nitrogen fixation in pure water. *J. Mater. Chem. A* 2019, *7*, 19831–19837.

[196] Wu, W. L.; Cui, E. X.; Zhang, Y.; Zhang, C.; Zhu, F.; Tung, C. H.; Wang, Y. F. Involving single-atom silver(0) in selective dehalogenation by AgF under visible-light irradiation. *ACS Catal.* 2019, *9*, 6335–6341.

[197] Collado, L.; Jansson, I.; Platero-Prats, A. E.; Perez-Dieste, V.; Escudero, C.; Molins, E.; I Doucastela, L. C.; Sánchez, B.; Coronado, J. M.; Serrano, D. P. et al. Elucidating the photoredox nature of isolated iron active sites on MCM-41. *ACS Catal.* 2017, *7*, 1646–1654.

[198] Lu, C.; Fang, R. Y.; Chen, X. Single-atom catalytic materials for advanced battery systems. *Adv. Mater.* 2020, *32*, 1906548.

[199] Sun, Y. W.; Zhou, J. Q.; Ji, H. Q.; Liu, J.; Qian, T.; Yan, C. L. Single-atom iron as lithiophilic site to minimize lithium nucleation overpotential for stable lithium metal full battery. *ACS Appl. Mater. Interfaces* 2019, *11*, 32008–32014.

[200] Zhai, P. B.; Wang, T. S.; Yang, W. W.; Cui, S. Q.; Zhang, P.; Nie, A. M.; Zhang, Q. F.; Gong, Y. J. Uniform lithium deposition assisted by single-atom doping toward high-performance lithium metal anodes. *Adv. Energy Mater.* 2019, *9*, 1804019.

[201] Du, Z. Z.; Chen, X. J.; Hu, W.; Chuang, C.; Xie, S.; Hu, A. J.; Yan, W. S.; Kong, X. H.; Wu, X. J.; Ji, H. X. et al. Cobalt in nitrogen-doped graphene as single-atom catalyst for high-sulfur content lithium-sulfur batteries. *J. Am. Chem. Soc.* 2019, *141*, 3977–3985.

[202] Zhang, L. L.; Liu, D. B.; Muhammad, Z.; Wan, F.; Xie, W.; Wang, Y. J.; Song, L.; Niu, Z. Q.; Chen, J. Single nickel atoms on nitrogen-doped graphene enabling enhanced kinetics of lithium-sulfur batteries. *Adv. Mater.* 2019, *31*, 1903955.

[203] Yang, T. Z.; Qian, T.; Sun, Y. W.; Zhong, J.; Rosei, F.; Yan, C. L.

[204] Zhang, B. W.; Sheng, T.; Liu, Y. D.; Wang, Y. X.; Zhang, L.; Lai, W. H.; Wang, L.; Yang, J. P.; Gu, Q. F.; Chou, S. L. et al. Atomic cobalt as an efficient electrocatalyst in sulfur cathodes for superior room-temperature sodium-sulfur batteries. *Nat. Commun.* 2018, *9*, 4082.

[205] Chu, T. S.; Rong, C.; Zhou, L.; Mao, X. Y.; Zhang, B. W.; Xuan, F. Z. Progress and perspectives of single-atom catalysts for gas sensing. *Adv. Mater.* 2023, *35*, 2206783.

[206] Li, Q. H.; Li, Z.; Zhang, Q. H.; Zheng, L. R.; Yan, W. S.; Liang, X.; Gu, L.; Chen, C.; Wang, D. S.; Peng, Q. et al. Porous γ-Fe_2O_3 nanoparticle decorated with atomically dispersed platinum: Study on atomic site structural change and gas sensor activity evolution. *Nano Res.* 2021, *14*, 1435–1442.

[207] Koga, K. Electronic and catalytic effects of single-atom Pd additives on the hydrogen sensing properties of Co_3O_4 nanoparticle films. *ACS Appl. Mater. Interfaces* 2020, *12*, 20806–20823.

[208] Xue, Z. G.; Yan, M. Y.; Yu, X.; Tong, Y. J.; Zhou, H.; Zhao, Y. F.; Wang, Z. Y.; Zhang, Y. S.; Xiong, C.; Yang, J. et al. One-dimensional segregated single au sites on step-rich ZnO ladder for ultrasensitive NO_2 sensors. *Chem* 2020, *6*, 3364–3373.

[209] Kim, Y.; Kang, S. K.; Oh, N. C.; Lee, H. D.; Lee, S. M.; Park, J.; Kim, H. Improved sensitivity in Schottky contacted two-dimensional MoS_2 gas sensor. *ACS Appl. Mater. Interfaces* 2019, *11*, 38902–38909.

[210] Yoon, H. J.; Jun, D. H.; Yang, J. H.; Zhou, Z. X.; Yang, S. S.; Cheng, M. M. C. Carbon dioxide gas sensor using a graphene sheet. *Sens. Actuat. B: Chem.* 2011, *157*, 310–313.

[211] Zheng, W.; Liu, X. H.; Xie, J. Y.; Lu, G. C.; Zhang, J. Emerging van der Waals junctions based on TMDs materials for advanced gas sensors. *Coord. Chem. Rev.* 2021, *447*, 214151.

[212] Zong, B. Y.; Xu, Q. K.; Mao, S. Single-atom Pt-functionalized $Ti_3C_2T_x$ field-effect transistor for volatile organic compound gas detection. *ACS Sens.* 2022, *7*, 1874–1882.

[213] Zhou, M.; Jiang, Y.; Wang, G.; Wu, W. J.; Chen, W. X.; Yu, P.; Lin, Y. Q.; Mao, J. J.; Mao, L. Q. Single-atom Ni-N_4 provides a robust cellular NO sensor. *Nat. Commun.* 2020, *11*, 3188.

[214] Ji, S. F.; Jiang, B.; Hao, H. G.; Chen, Y. J.; Dong, J. C.; Mao, Y.; Zhang, Z. D.; Gao, R.; Chen, W. X.; Zhang, R. F. et al. Matching the kinetics of natural enzymes with a single-atom iron nanozyme. *Nat. Catal.* 2021, *4*, 407–417.

[215] Jiao, L.; Xu, W. Q.; Zhang, Y.; Wu, Y.; Gu, W. L.; Ge, X. X.; Chen, B. B.; Zhu, C. Z.; Guo, S. J. Boron-doped Fe-N-C single-atom nanozymes specifically boost peroxidase-like activity. *Nano Today* 2020, *35*, 100971.

[216] Sun, L. P.; Li, W. Q.; Liu, Z. H.; Zhou, Z. J.; Feng, Y. Iodine-doped single-atom cobalt catalysts with boosted antioxidant enzyme-like activity for colitis therapy. *Chem. Eng. J.* 2023, *453*, 139870.

[217] Zhu, Y.; Wang, W. Y.; Cheng, J. J.; Qu, Y. T.; Dai, Y.; Liu, M. M.; Yu, J. N.; Wang, C. M.; Wang, H. J.; Wang, S. C. et al. Stimuli-responsive manganese single-atom nanozyme for tumor therapy via integrated cascade reactions. *Angew. Chem., Int. Ed.* 2021, *60*, 9480–9488.

[218] Chen, Y. J.; Jiang, B.; Hao, H. G.; Li, H. J.; Qiu, C. Y.; Liang, X.; Qu, Q. Y.; Zhang, Z. D.; Gao, R.; Duan, D. M. et al. Atomic-level regulation of cobalt single-atom nanozymes: Engineering high-efficiency catalase mimics. *Angew. Chem., Int. Ed.*, in press, https://doi.org/10.1002/anie.202301879.

[219] Yang, M.; Liu, J. L.; Lee, S.; Zugic, B.; Huang, J.; Allard, L. F.; Flytzani-Stephanopoulos, M. A common single-site Pt(II)-O(OH)$_x$-species stabilized by sodium on "active" and "inert" supports catalyzes the water-gas shift reaction. *J. Am. Chem. Soc.* 2015, *137*, 3470–3473.

[220] Yang, M.; Allard, L. F.; Flytzani-Stephanopoulos, M. Atomically dispersed Au-(OH)$_x$ species bound on titania catalyze the low-temperature water–gas shift reaction. *J. Am. Chem. Soc.* 2013, *135*, 3768–3771.

[221] Lin, J.; Wang, A. Q.; Qiao, B. T.; Liu, X. Y.; Yang, X. F.; Wang, X. D.; Liang, J. X.; Li, J.; Liu, J. Y.; Zhang, T. Remarkable

performance of Ir_1/FeO_x single-atom catalyst in water gas shift reaction. *J. Am. Chem. Soc.* **2013**, *135*, 15314–15317.

[222] Studt, F.; Abild-Pedersen, F.; Bligaard, T.; Sørensen, R. Z.; Christensen, C. H.; Nørskov, J. K. Identification of non-precious metal alloy catalysts for selective hydrogenation of acetylene. *Science* **2008**, *320*, 1320–1322.

[223] Bu, J.; Liu, Z. P.; Ma, W. X.; Zhang, L.; Wang, T.; Zhang, H. P.; Zhang, Q. Y.; Feng, X. L.; Zhang, J. Selective electrocatalytic semihydrogenation of acetylene impurities for the production of polymer-grade ethylene. *Nat. Catal.* **2021**, *4*, 557–564.

[224] Liu, Y. X.; Liu, X. W.; Feng, Q. C.; He, D. S.; Zhang, L. B.; Lian, C.; Shen, R. A.; Zhao, G. F.; Ji, Y. J.; Wang, D. S. et al. Intermetallic Ni_xM_y (M = Ga and Sn) nanocrystals: A non-precious metal catalyst for semi-hydrogenation of alkynes. *Adv. Mater.* **2016**, *28*, 4747–4754.

[225] Chan, C. W. A.; Mahadi, A. H.; Li, M. M. J.; Corbos, E. C.; Tang, C.; Jones, G.; Kuo, W. C. H.; Cookson, J.; Brown, C. M.; Bishop,

P. T. et al. Interstitial modification of palladium nanoparticles with boron atoms as a green catalyst for selective hydrogenation. *Nat. Commun.* **2014**, *5*, 5787.

[226] Fu, X. B.; Liu, J.; Kanchanakungwankul, S.; Hu, X. B.; Yue, Q.; Truhlar, D. G.; Hupp, J. T.; Kang, Y. J. Two-dimensional Pd rafts confined in copper nanosheets for selective semihydrogenation of acetylene. *Nano Lett.* **2021**, *21*, 5620–5626.

[227] Liu, Y. W.; Wang, B. X.; Fu, Q.; Liu, W.; Wang, Y.; Gu, L.; Wang, D. S.; Li, Y. D. Polyoxometalate-based metal-organic framework as molecular sieve for highly selective semi-hydrogenation of acetylene on isolated single Pd atom sites. *Angew. Chem., Int. Ed.* **2021**, *60*, 22522–22528.

[228] Gao, R. J.; Xu, J. S.; Wang, J.; Lim, J.; Peng, C.; Pan, L.; Zhang, X. W.; Yang, H. M.; Zou, J. J. Pd/Fe_2O_3 with electronic coupling single-site Pd–Fe pair sites for low-temperature semihydrogenation of alkynes. *J. Am. Chem. Soc.* **2022**, *144*, 573–581.